Energy & Buildings 324 (2024) 114926

Contents lists available at ScienceDirect

Energy & Buildings

journal homepage: www.elsevier.com/locate/enb

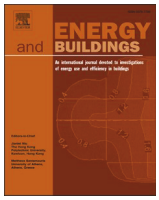

Dual impacts of solar-reflective façades in high-density urban areas on building energy use and outdoor thermal environments

Chenshun Chen [a], Julian Wang [a,*], Huijin Zhang [b], Xinyue Xu [a], Laura Elizabeth Hinkle [a], Xiao Chao [b], Qian Shi [b]

[a] Department of Architectural Engineering, Pennsylvania State University, United States
[b] School of Economics and Management, Tongji University, China

ARTICLE INFO

Keywords:
Building façade
Building energy
Urban heat island
Microclimate
Heat stress
Solar radiation

ABSTRACT

In the context of rising urban temperatures, this investigation delves into the impacts of solar reflectance on glazed facades, shedding light on urban microclimates and the resulting thermal experiences. Recent retrofit strategies have employed low emissivity and high solar reflective materials to enhance energy efficiency and indoor comfort against climbing outdoor temperatures. Despite these advances, adverse effects on outdoor heat conditions are often reported due to the intrinsic relationships among the glazed facades' optical and thermal properties, highlighting a gap in thorough, quantitative assessments in this domain. Accordingly, this study aims to bridge this gap, examining the comprehensive effects of glazed facades' solar reflectance on building energy performance and the Universal Thermal Climate Index (UTCI) in densely populated urban settings. Utilizing computational simulations and empirical analysis, we scrutinized changes in outdoor solar radiation, ground temperature, UTCI, and building-specific energy demands, including heating, cooling, and lighting energy use, correlating these with varying façade's solar reflectance levels during peak summer periods. Results affirm the potential of highly solar reflective facades to substantially cut cooling energy needs by mitigating solar heat gain and thermal conductance. However, a notable byproduct is the upsurge in UTCI, signaling increased heat stress risk within urban canyons. Our comprehensive, multi-objective optimization approach seeks to harmonize the solar reflectance of facades, aiming to reconcile energy conservation with the imperative of maintaining urban thermal comfort. This research contributes significantly to urban retrofit strategies and also guides the potential sustainable urban and landscape design that harmonizes urban energy savings with the mitigation of urban heat implications.

1. Introduction

With the increasing frequency of extreme weather events in recent years, the influence of urban building environments and ongoing building energy retrofit practices on the microclimate has garnered heightened attention. This attention is particularly relevant in the context of the Urban Heat Island (UHI) effect, which is defined as the rise in temperature in any man-made area, which results in a well-defined, distinct "warm island" of urban area among the surrounding natural landscape [1]. The adverse effects of UHI include degradation of the living environment, increase in energy consumption, elevation in ground-level ozone, and even an increase in mortality rates [2]. Two major sources induce the temperature increase in an urban area: solar irradiation, encompassing both direct sunlight and its indirect effects via reflection and re-radiation from urban and building structures, and anthropogenic heat from human activities and air pollutants. Building facades or envelopes play a crucial role in this context due to their interaction with solar irradiation impacting the outdoor environment. This impact is particularly pronounced in dense areas where the characteristics of building facades are more influential. There have been reports and discussions in different channels indicating that highly reflective building surfaces and windows may significantly influence the outdoor thermal environment. One study found that an increase in surface reflectance in simple urban canyons adversely affects outdoor thermal comfort due to increased surface temperature: PET temperatures can increase up to 5.6 °C during the hottest hour of the day, with high road and façade reflectivity. However, when lowering the façade reflectivity, urban canyon PET temperature can have a reduction of up to 1.6 °C [3]. Another research indicated that using high albedo

* Corresponding author at: Department of Architecture Engineering, The Pennsylvania State University, University Park, PA 16802, United States.
E-mail address: jqw5965@psu.edu (J. Wang).

https://doi.org/10.1016/j.enbuild.2024.114926
Received 26 March 2024; Received in revised form 6 October 2024; Accepted 15 October 2024
Available online 19 October 2024

Nomenclature

UHI	Urban Heat Island
UTCI	Universal Thermal Comfort Index
T_a	Dry-bulb air temperature (°C)
T_{mrt}, MRT	Mean Radiant Temperature (°C)
V_a	Air Velocity (m/s)
GH	Grasshopper
DF	Grasshopper, Dragonfly plug-in
HB	Grasshopper, Honeybee plug-in
LB	Grasshopper, Ladybug tools
SHGC	Solar Heat Gain Coefficient
R_{fsol}	Façade front solar reflectance
BRTD	Bidirectional Reflection and Transmission Distribution
EUI	End Use Intensity (kWh/m^2)

materials in urban areas could contribute to a worsening outdoor thermal environment [4]. In addition to academic research, there have been real-world instances highlighting the adverse effects of reflective building materials. Notably, the Vdara Hotel in Las Vegas experienced a phenomenon dubbed the "Death Ray," where the hotel's glass façade concentrated sunlight to such an extent that it heated the hotel pool area and reportedly melted plastic items [5]. Similarly, in residential neighborhoods, the reflective properties of solar-heat-control Low-E facades have been known to focus sunlight onto neighboring houses, causing the vinyl siding to warp and melt [6]. These incidents illustrate the practical implications of reflective surfaces in dense environments, where concentrated solar reflections can lead to unintended and potentially hazardous consequences.

Concurrently, there is an ongoing emphasis on energy-efficient design and energy retrofitting of these envelopes. To mitigate the potential heatwave impacts, significant efforts have been made in designing or retrofitting solar-reflective facades to boost energy efficiency and improve indoor thermal comfort. A notable example is the widespread use of Low-E coatings in fenestration systems, especially those with a low solar heat gain coefficient (SHGC) in hotter climates. These coatings are solar-reflective, allowing most visible light to pass through while reflecting a significant portion of solar infrared radiation (heat). *Somasundaram et al.* reported the potential HVAC energy saving by the combination installation of solar film (i.e., Low-E film) with retrofit double glazing up to 20 % 7. The global market for Low-E Glass estimated at US$45.3 Billion in the year 2020, is projected to reach a revised size of US$88 Billion by 2027 [8]. With the development of novel window systems, for example, Phase Change Material (PCM) film (such as VO_2 [9]) and complex-structured smart window systems (such as windows integrated with thermotropic parallel slat-transparent insulation material [10]), building energy reduction can be even higher with the un-compromising indoor luminous environment [11]. Other technologies include NIR-selective coatings for envelopes [12], passive cooling pigments/paintings [13], heat-mirror panels, etc. As these types of high-reflective materials and solar-control technologies become more popular for energy efficiency and thermal resilience enhancement purposes, their impacts on urban microclimates draw increasing attention from researchers. Salvati *et al.* investigated the impacts of reflective materials on urban canyon albedo, and outdoor and indoor microclimates, and they found that increasing surface reflectance in urban canyons has a detrimental impact on outdoor thermal comfort [3]. Yuan *et al.* found that a highly reflective façade would increase the amount of solar radiation and heat flux reflected to the urban canyon, and the outdoor air temperature of the specular reflective (SR) façade was about 0.04 °C and 0.13 °C higher than that of the *retro*-reflective (RR) and the diffuse highly reflective (DHR) façade, respectively [14]. Martins *et al.* showed that by increasing all surfaces of the surrounding building's albedo to 0.9, the average Physiological Equivalent Temperature (PET) was increased by 1 °C [15]. Mehaoued *et al.* examined the influence of the reflective glass façade of an office building on its surrounding microclimate and building cooling load in Algiers, and it was found that the air temperature surrounding the building significantly increased due to the multiple reflections of the radiation heat flux, which leads to an increase in the cooling demand [16]. Wen *et al.* conducted field measurements for a school building in Singapore that was affected by a surrounding highly reflective stainless-steel façade, and the results showed that the surrounding highly reflective façade incurred both outdoor solar radiation and outdoor air temperature, which in turn affected the school's indoor illuminance and air temperature [4]. A more recent study targeted the impact of a specific component: building window systems (i.e., window reflectivity and size). They examined 40 scenarios by employing ENVI-met model, and simulation results revealed their spatiotemperal characteristics (i.e., windows' impacts was time- and spatial- dependent) and intrinsic interaction (between window size and reflectivity) [17]. *Other* studies showed that reflective facades affected outdoor surface temperature, thereby affecting outdoor thermal comfort [17,18]. In brief, considering envelope energy-efficient retrofit and thermal resilience, a variety of innovative materials and technologies are proving highly effective in boosting both the energy efficiency and thermal resilience of individual buildings [19], while some envelope retrofit options with high solar-reflective characteristics may increase the inter-reflections between surrounding buildings and harm the outdoor urban microenvironment.

In summary, there is a general agreement that the application of solar-reflective materials on building facades requires careful consideration from both research and practical standpoints. While prior studies have focused on a single building's surface reflectance on its surrounding environment and building energy demand, or city-scaled analysis with less-detailed materials properties, it remains unclear how building façade impacts the urban microclimate and building energy demand on a mesoscale, by taking dense urban structure (i.e., the interactions between numerous building facades) and the complex glazed façade optical and thermal properties (e.g., most studies only considered surface albedo, neglecting the intrinsic relationships among glazed facades' solar reflectivity, solar heat gain coefficient, thermal transfer coefficient, and visible transmittance.) into consideration at the same time. Therefore, a more comprehensive workflow should be established integrating urban microclimate modeling, building energy modeling, and glazed façade characterizations to quantitatively analyze the interactions between solar-reflective façade, outdoor thermal environment, and building energy consumption, within dense urban areas. Further, this research raises another important query: can we achieve a balance between reducing building energy use and mitigating adverse effects on outdoor thermal comfort? The key may lie in optimizing the properties of external wall surfaces, particularly in densely built urban areas, to harmonize energy efficiency with environmental impact.

From the perspective of research contribution to the new body of knowledge, this investigation pioneers the analysis of the nexus between building envelope retrofits and their concurrent effects on energy use and outdoor thermal environments within a specific urban typology characterized by the predominant use of glass in high-rise building facades. Through an integrative suite of numerical modeling, computational simulations, and a substantiated case study enhanced by comprehensive data analytics, this research scrutinizes the dual impact of NIR-reflective façade materials in such urban center contexts. Our methodological innovation bridges simulation with optimization, yielding new insights into façade material design and its engineering implications in those densely urbanized areas featuring high-rise glazed façades. This study's rigorous examination of solar-reflective facades marks an important understanding of their influence on both microclimatic thermal conditions and building energy profiles. Specifically, it informs the escalating discourse on reconciling the objectives of sustainability with the imperatives of thermal resilience, particularly as

NIR-reflective technologies become central to energy-efficient building design. The insights gleaned here are set to steer policy-making and architectural practices towards a synergistic balance between green building initiatives and urban thermal adaptability.

2. Related work about façade impacts on urban thermal environments

The correlation between building facades and urban microclimate has been the topic of ongoing research and development in recent years. Past studies mainly took two approaches to unveil this underlying correlation: either through field measurements (unmanned aerial vehicles (UAVs), remote sensing, local weather station, etc.) or computational techniques, depending on the ambient levels (surface layer, canopy layer, and boundary layer), analysis scales (mesoscale, local-scale or microscale) and quantifiable parameters (land surface temperature, surface temperature, air temperature, sky view factor (SVF), physiology equivalent temperature (PET), etc.) [20,21]. For example, to investigate how reflective materials affect the urban microclimate, many researchers took field measurements by using the micro-weather station, radiometer, thermometers, thermocouples, etc. to gauge the spatial–temporal radiative flux, air temperature, surface temperature, and other meteorological parameters for further analysis [3,4]. However, such field campaigns are limited by the time-span and location of measured data, therefore they are more suitable for model validation, especially in large-scaled scope. On the other hand, computer simulations have the advantage of reporting spatial–temporal results on large-scale areas. Many researchers have done building façade-urban microclimate studies with the aid of computational tools [16,17,22], according to *Mirzaei et al.*'s review paper on the recent urban microclimate modeling studies [23], there are mainly three paths: 1). Using airflow (i.e., meso and micro-scale CFD) and energy balanced (i.e., Urban canopy model (UCM) and building energy model (BEM)) for UHI intensity and building energy load analysis [24,25]; 2). Evaluating a thermal comfort index (such as PET, UTCI) to study the impacts of different UHI intensities on human comfort [26]; 3). Using remote sensing data incorporated with machine learning tools to evaluate the effects of urban characteristics on UHI spatial–temporal variation [27,28]. In our case, mesoscale building models (using BEM tools such as EnergyPlus) with the integration of Radiance, CFD, and UCM would be suitable for studying the effects of different solar-reflective facades on outdoor thermal environments. As for the simulation tool, there exists two major

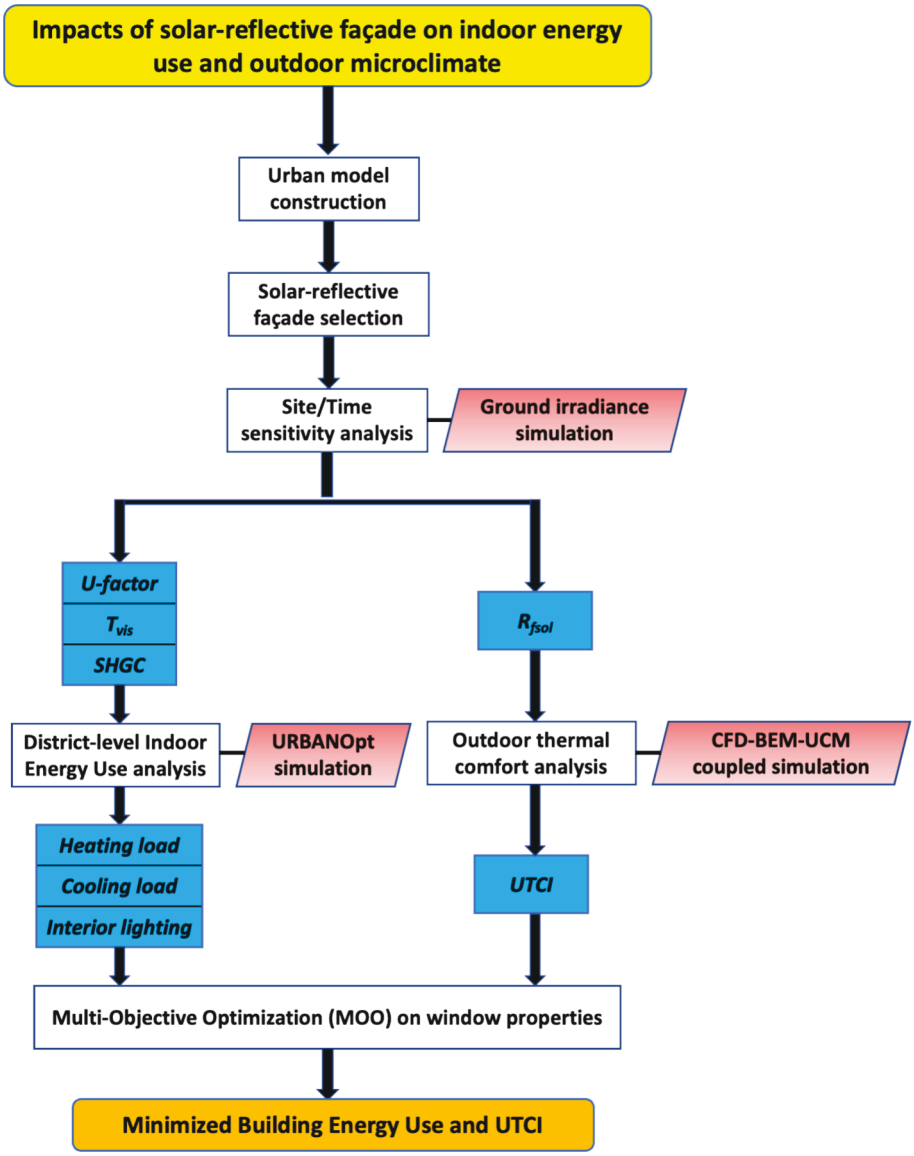

Fig. 1. Diagram of the computational analysis workflow used in this work.

types: Energy Balance Models (EBM)-based models, such as RayMan, SOLWEIG, TEB, and Computational Fluid Dynamic (CFD)-based models such as OpenFOAM, FLUENT, STAR-CCM+, PHOENICS, ENVI-met [29,30]. CFD can produce more accurate information within and above building canopies compared to the EBM models (as an approximation of heat fluxes using empirical correlations in UCM models rarely captivate the interaction between velocity and temperature fields), but it also brings computational and theoretical challenges. To balance the accuracy and complexity of our model, a novel workflow developed in the Grasshopper environment was adopted, where Ladybug tools are used to model the mutual relations amongst urban microclimate, building energy performance, and outdoor thermal comfort [22]. To understand the problem from a thermal comfort perspective, the UTCI index is also generated by taking both meteorological and physiological parameters into consideration.

3. Methodology

In this research, we employed a systematic numerical approach coupled with a case study to assess the effects of solar-reflective facades, which is illustrated in Fig. 1 above. The initial step in our methodology was the construction of an urban model. Utilizing Elk, a plugin for Grasshopper, we created a detailed representation of the Logan Square area in Central Philadelphia, PA, USA. This urban model built with the URBANOpt platform served as the basis for our simulations and further analysis. Following the urban modeling, our investigation is carried out in three phases. To potentially reveal the significant trade-off, we expected to focus on the façade impacts on hot summer situations and specific or sensitive locations in the urban area. Therefore, ***in the first phase***, we particularly modeled high solar reflectance façade conditions and then used Honeybee Radiance to map solar irradiation levels in the selected urban area under a few selected hot summer days. Through this step, the sensitivity of which parts of the urban and what time/weather conditions were obtained. ***In the second phase***, we conducted a series of simulations with two major pathways. On the one hand, we conducted district-level urban energy simulations, considering factors such as heating and cooling loads and interior lighting demands. On the other hand, we analyzed thermal comfort levels outdoors by implementing the Universal Thermal Climate Index (UTCI) as our metric, utilizing the LB UTCI tool to generate comprehensive UTCI maps. Through this phase, we obtained two sets of responses – in terms of building energy use and outdoor UTCI values with different façade solar properties. ***The last phase*** was to conduct correlation analyses between the façade solar reflectance and two key responses, and further perform optimization analysis to determine the optimal façade properties for best energy performance and minimal urban heat impacts.

3.1. Location, climate, and urban modeling

For our analysis, we selected Philadelphia, PA, USA, and its urban central area – Logan Square, 392 m × 312 m (121,604 m^2, shown in Fig. 2), as the basic yet realistic urban context for our analysis. Specifically, we utilized Elk, a Grasshopper plugin, to create a detailed model of this dense urban area. Elk is adept at generating topographies and street maps, leveraging data from OpenStreetMap.org and the Shuttle Radar Topography Mission (SRTM) provided by NASA/Jet Propulsion Laboratory [31]. Philadelphia, PA has been experiencing an uptick in the frequency and intensity of heatwave events. Recent data analysis suggests that the city currently faces three-day stretches of dangerous heat more regularly. This increase in heatwave events is particularly more pronounced in urban areas due to the urban heat island effect, where built environments contribute to higher temperatures compared to rural areas. Local initiatives, such as the "Beat the Heat" and "Heat Response" projects [32], involve community engagement in areas like Fairhill, Grays Ferry, and Southeast Philadelphia to create public art that raises awareness and addresses the UHI effect. The city has also developed the Philadelphia Heat Vulnerability Index (HVI) [33], which highlights key factors associated with the adverse health effects of extreme heat events, indicating a focused approach to tackling heat-related challenges in urban settings (Fig. 3).

The urban model contains three types of buildings, streets, sidewalks, and leisure/open information in the Logan Square area, Philadelphia. To simplify the model, the following assumptions were made:

- All building blocks were simply extruded as boxes without any complex shapes, shades, or attachments.
- Three building types were assigned according to their general functionality: large office, high-rise apartment, and primary school.
- Ground zones had been pruned to have only three types, leisure areas, sidewalks, and roads.
- Vegetations in the urban area have been neglected (which might have a large impact on the simulation results since vegetation can help mitigate the UHI effect by providing shade, evaporative cooling, and reducing the amount of solar radiation absorbed by surfaces [35–37]).

All building blocks were created as Dragonfly (DF)-Building components, with a uniform story height of 8 m (which is unrealistic but would help reduce the computational load). Then these DF objects could either be used directly by Urban Weather Generator (UWG), or they could also be converted to Honeybee (HB) objects (within which each story was an HB-Room component), and be used in Radiance or Building Energy Modeling (BEM). Apertures were then assigned to these HB-Rooms, with uniform Window-Wall Ratio (WWR): 80 % for large offices, 60 % for high-rise apartments, and 40 % for primary school. HB-Ground rooms were also created and applied to the HB model, to

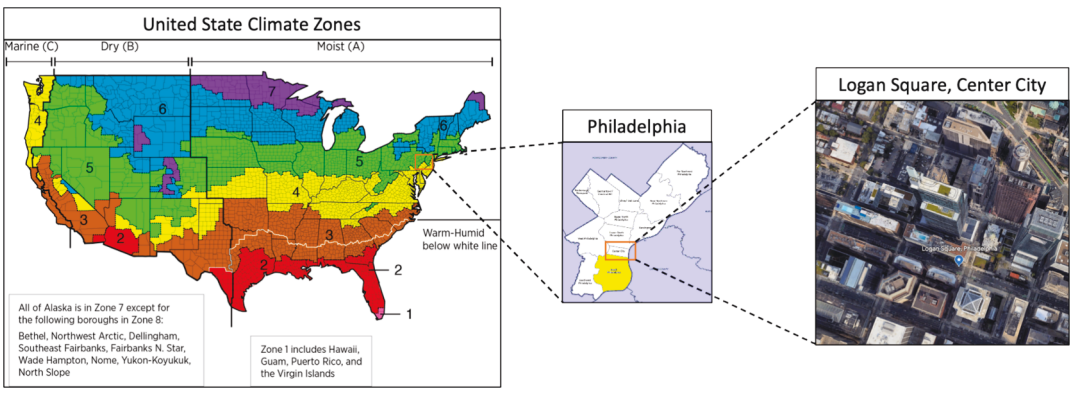

Fig. 2. Urban model location: Logan Square, Central Philadelphia.

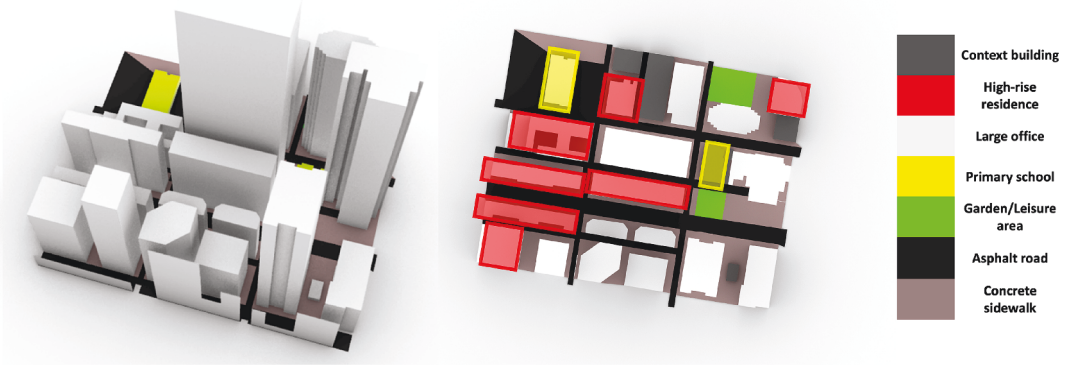

Fig. 3. Urban model in Rhinoceros 3D format (Top: Snapshot of Logan Square, Philadelphia from Google Earth [34]; Bottom: Top & perspective view of Rhino 3D model).

account for different types of ground components.Ground materials' thermal and optical properties are shown in appendix Table 1-s. Fig. 4 shows the rendering view of the 3D urban model. After all these steps, the DF/HB model was ready for UHI, energy, and radiance simulations, which could help quantify the impacts of solar-reflective façade on indoor and outdoor environments from different perspectives.

3.2. Solar irradiation analysis method

The key aspect under study is how different façades influence ground-level solar irradiance. For this, a Radiance-based two-phase method was utilized, comparing two façade systems: a standard double-pane glazed façade (solar reflectance 0.1) and one with low emissivity coatings (solar reflectance 0.7). The properties of these façades were adjusted using Radiance Glass Modifiers and the BRTD function, focusing on the directionality of transmitted and reflected rays. Radiance's BRTDfunc gives maximum flexibility over surface reflectance and transmittance, providing for spectrally-dependent specular rays, reflectance, and transmittance distribution functions [38]. Despite the availability of detailed solar spectrum data from the IGDB database, this study simplifies the approach by assuming constant RGB transmittance/reflectance across the solar spectrum (i.e., RGB transmittance/reflectance are all equal to T_{sol} and R_{fsol} in Table 1). It should be noticed that such simplification may underestimate the effects of glazed façade's reflectance (especially with Low-E coatings) on outdoor solar conditions, as such solar control measures tend to reflect more solar radiation in the near-infrared region, compared to traditional glazing materials [39].

In order for this method to work, the ambient interpolation has to be switched off (i.e., −aa 0, −as 0, −ar 0), giving rise to noise results and requiring a higher number of ambient divisions (−ad). Other parameters such as ambient bounces (−ab) would also have a great influence on our study, the value will affect the rays that reach the ground (especially in such a dense urban area), as illustrated by the Ray-tracing diagram shown in Fig. 5. As for the analysis period, it is reasonable to infer that solar-reflective façade would have a greater influence on indoor and outdoor environments during extreme weather conditions (e.g., heatwaves), when sky condition was clear, DNI was high, and under certain sun direction. Therefore, the middle day during a heatwave period (defined as 2 + consecutive days when maximum daily temperatures are 90°F or higher [40]): 9:00 AM – 17:00 PM, Aug 18th (with a minimum DNI of 672 W/m^2 and maximum total sky cover of 20 %), were simulated and compared to see if sun directions and solar irradiance level had impacts on ground irradiance near high solar-reflective façade. The grid size of the receiving surface is set to be 5.0 m.

3.3. Computation of detail façade properties

To thoroughly examine the effects of solar-reflective facades and their relationship with energy consumption and the outdoor environment, we developed and analyzed 25 different glazed façade models. These models were simulated using the LBNL OPTICS and WINDOW

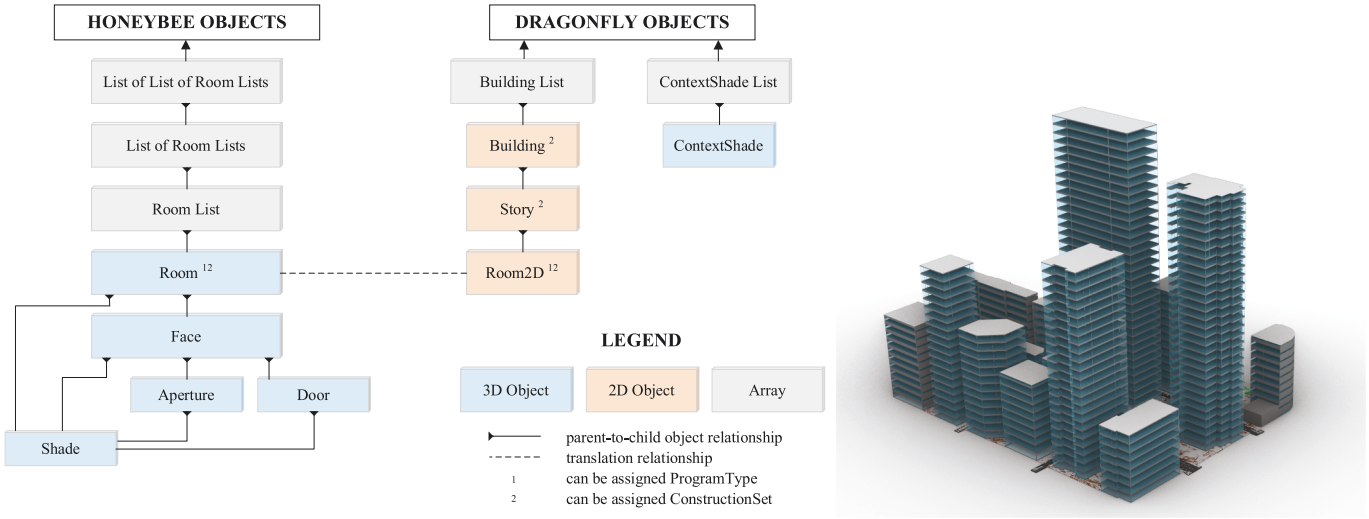

Fig. 4. DF/HB model conversion rule and finalized energy model ready for simulations.

Table 1
Detailed glazing façade properties.

Glazed Façade ID	T_{vis}	SHGC	U-factor (W/m^2·K)	R_{fsol}	T_{sol}	Abs1
1 (Baseline)	**0.78**	**0.70**	**2.54**	**0.11**	**0.61**	**0.17**
2	0.77	0.68	2.52	0.13	0.58	0.19
3	0.77	0.66	1.95	0.15	0.59	0.15
4	0.74	0.62	1.82	0.17	0.55	0.15
5	0.61	0.59	1.78	0.20	0.29	0.16
6	0.76	0.58	1.46	0.23	0.48	0.23
7	0.79	0.57	1.39	0.25	0.49	0.18
8	0.78	0.56	1.39	0.27	0.49	0.17
9	0.73	0.47	1.37	0.30	0.34	0.20
10	0.71	0.46	1.37	0.33	0.33	0.20
11	0.70	0.46	1.37	0.35	0.41	0.07
12	0.69	0.42	1.36	0.37	0.30	0.21
13	0.69	0.39	1.36	0.39	0.26	0.22
14	0.60	0.35	1.35	0.43	0.23	0.22
15	0.57	0.32	1.35	0.45	0.22	0.22
16	0.55	0.31	1.35	0.47	0.22	0.22
17	0.51	0.28	1.35	0.50	0.19	0.23
18	0.44	0.26	1.35	0.52	0.20	0.22
19	0.42	0.25	1.35	0.54	0.21	0.24
20	0.40	0.24	1.35	0.56	0.24	0.18
21	0.39	0.23	1.35	0.58	0.22	0.17
22	0.38	0.22	1.35	0.61	0.27	0.09
23	0.36	0.21	1.34	0.64	0.17	0.19
24	0.27	0.19	1.34	0.67	0.14	0.21
25	**0.25**	**0.17**	**1.33**	**0.70**	**0.14**	**0.14**

software, incorporating data from the IGDB library. For facades with enhanced solar reflectivity, Low-E films were applied to the rear surface of the first layer. Notably, although most ultra-low Low-E coated windows have strong solar reflectivity, there are still considerable Low-E products with minimal solar reflection features. In general, hard-coated Low-E products are more commonly applied for commercial building curtain walls or glazed façades due to their durability and resistance to damage. However, they typically result in higher solar reflectivity and lower solar heat gains. In this study, to streamline our approach and align with common practices in our selected city, we specifically concentrate on Low-E glazings sourced from the IGDB library that have solar heat control capabilities. In particular, the baseline model consisted of double-pane clear glazing materials, characterized by high solar light transmittance but low front solar reflectance. In contrast, the comparative models were designed using coated glazed facades. As shown in Table 1, these models progressively increased the front solar reflectance by changing the Low-E coatings from high levels to ultra-low conditions. Previous research has consistently shown that glazed façades featuring lower emittance coatings generally exhibit lower Solar Heat Gain Coefficient (SHGC) values, due to their increased front solar reflectance. At the same time, the U-factor, which measures heat transfer, and visible transmittance, which relates to the amount of visible light that passes through, are also significantly influenced by the presence and type of low-e coatings. It should be noted that although OPTIC and WINDOW are capable of calculating the angular and spectral properties of glazing assemblies, they were assumed to be angularly and spectrally independent. These normal incidence, spectral-averaged optical, and thermal properties were then inserted into simulations and acted as control variables for future optimization.

There are four key factors in the simulation and optimization processes, including SHGC, U-factor, and T_{vis} and R_{fsol}. Among these parameters, SHGC and U-factor primarily affect buildings' heating and cooling loads, while T_{vis} will affect buildings' interior artificial lighting (with the implementation of daylight control strategy and dimmable lights), therefore building energy use is dependent on these variables. On the other hand, R_{fsol} determines the amount of solar energy that will be re-directed to the outside by these glazed façade systems, therefore, the outdoor thermal environment will be primarily affected by this parameter. Modeled glazed façade properties are listed in Table 1, from which their properties have shown some patterns: from baseline model to high solar-reflective model, R_{fsol} keeps increasing from 0.11 to 0.70, with an approximate interval of 0.02; SHGC and U-factor have opposite trends compared with R_{fsol}, as they decrease when R_{fsol} increases (i.e., negatively correlated), and linear regression shows the following relationship between SHGC/U-factor and R_{fsol} ($R^2 = 0.9785$):

$$R_{fsol} = -1.08*SHGC + 0.032*U_{fator} + 0.789 \quad (1)$$

Other parameters such as the glazed façade's first layer absorptance (Abs1) may affect the façade's surface temperature, which in turn affects outdoor longwave mean radiant temperature (Longwave MRT) calculation. It should be noticed that according to the International Energy Conservation Code 2018 (IECC 2018) [41], for commercial building energy efficiency in climate zone 4, building envelope fenestration should have a maximum U-factor 0.38 BTU/hr·ft^2·°F (approximately 2.16 W/m^2·K) and SHGC 0.36/0.48 (for Projection Factor <0.2, orientations other than North/North-facing). The purpose of including those samples with relatively higher U-factor and SHGC in this work was

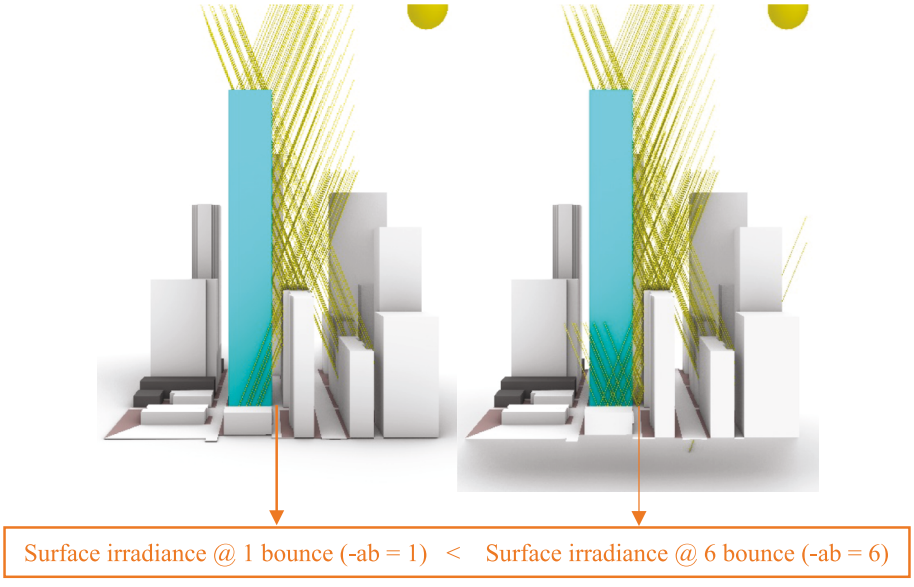

Fig. 5. Ray-tracing diagram of Radiance model (Left: single ambient bounce/reflection; Right: 6-times ambient bounce/reflection).

mainly for the underlying relationship analysis rather than energy performance examination.

3.4. District-level building energy use estimation method

After determining the most sensible time and area of this study, the next step is to find out how solar-reflective façade could affect indoor building energy use, especially for cooling during hot summer days. To perform a district-level urban energy simulation, we utilized the URBANOpt (or Urban Renewable Building and Neighborhood Optimization) platform developed by the National Renewable Energy Laboratory (NREL). By integrating with other simulation tools, such as EnergyPlus and OpenStudio, URBANopt offers detailed building energy modeling and analysis. Its flexibility allows users to assess different combinations of building materials, constructions, and systems, as well as district-level energy infrastructure, such as district heating and cooling networks or microgrids. Honeybee and Dragonfly toolkits in Rhino were used to build up the URBANOpt simulation. The detailed workflow schema is shown in Fig. 6 [42].

The focused simulating area was the lower half of the urban model, as shown in Fig. 7. Each story of each target building represents a thermal zone within the building energy simulations. Different buildings were adopting different programs based on their functionality, with default ASHRAE 90.1 2019, ClimateZone 4, SteelFramed construction sets (except for window construction sets). Detailed information is shown in Table 2-s in the Supplementary material. Then different glazed façade constructions (modified U-factor, SHGC, and T_{vis}) were assigned to the target buildings to simulate the district-level building energy use intensity (EUI) under different R_{fsol} levels. There are three varying end users in the final EUI results: heating, cooling, and interior lighting. For heating and cooling, all buildings adopted the 'Ideal Load Air System' as an HVAC template, which calculates the exact heating and cooling demands. For interior lighting, lighting power density (LPD) was set as 6.66 W/m^2, 8.86 W/m^2, and 7.18 W/m^2, for office, apartment, and primary school buildings, respectively, according to ASHRAE 2019 standards. As URBANOpt itself could not perform a daylight control strategy, an OpenStudio Measure 'Reduce Lighting Loads By Percentage' was implemented. To estimate the reducing percentage for different glazed façade constructions, a simplified method proposed by *Krarti et al.* was used [43]:

$$f_d = 73[(1 - exp(-7\tau_w A_w/A_p)]\frac{A_p}{A_f} \quad (2)$$

which, f_d is the percentage of artificial lighting energy saving through the use of daylighting, τ_w is the glazed façade system's visible transmittance, A_w is the total glazed façade area for the building, A_p is the total perimeter floor area (i.e., daylit floor area, based on a room depth of 12 ft) and A_f is the total floor area of the building. For office buildings, the total floor area A_f is 404,481 m^2, the total glazed façade area A_w is 219,394 m^2, and the total perimeter area is assumed to be 30 % of the total floor area (which is 121,344 m^2); For apartment buildings, the total floor area A_f is 20,446 m^2, the total glazed façade area A_w is 72,283 m^2, and the total perimeter area is assumed to be 50 % of the total floor area (which is 100,223 m^2); For school buildings, the total floor area A_f is 3,264 m^2, the total glazed façade area A_w is 1,007 m^2, and the total perimeter area is assumed to be 20 % of the total floor area (which is 653 m^2). It should be noted that this method can only estimate the rough reduction of electric lighting energy, as a detailed daylight control strategy should use more advanced tools such as Radiance to estimate the accurate daylight-saving potential of using a transparent façade. The output values from the URBANOpt simulation will be Energy Use Intensity (EUI in units: kWh/m^2). By comparing the results listed above, the impacts of solar-reflective façade on building energy use can be quantified, and optimized in the future.

3.5. Outdoor thermal environment assessment method

Another important optimizing objective for our study is outdoor thermal comfort. In this study, the Universal Thermal Climate Index (UTCI) was adopted as the variable for quantifying outdoor thermal comfort levels. UTCI is the equivalent temperature for the environment derived from a reference environment. It is defined as the air temperature of the reference environment which produces the same strain index value in comparison with the reference individual's response to the real environment [44]. As one of the most comprehensive indices for calculating heat stress in outdoor spaces [45], UTCI calculates the offset (i.e., the deviation of UTCI from air temperature) by taking both meteorological and non-meteorological (metabolic rate and clothing thermal resistance) into consideration, as shown in Fig. 8 [46,47].

The meteorological parameters that are taken into consideration

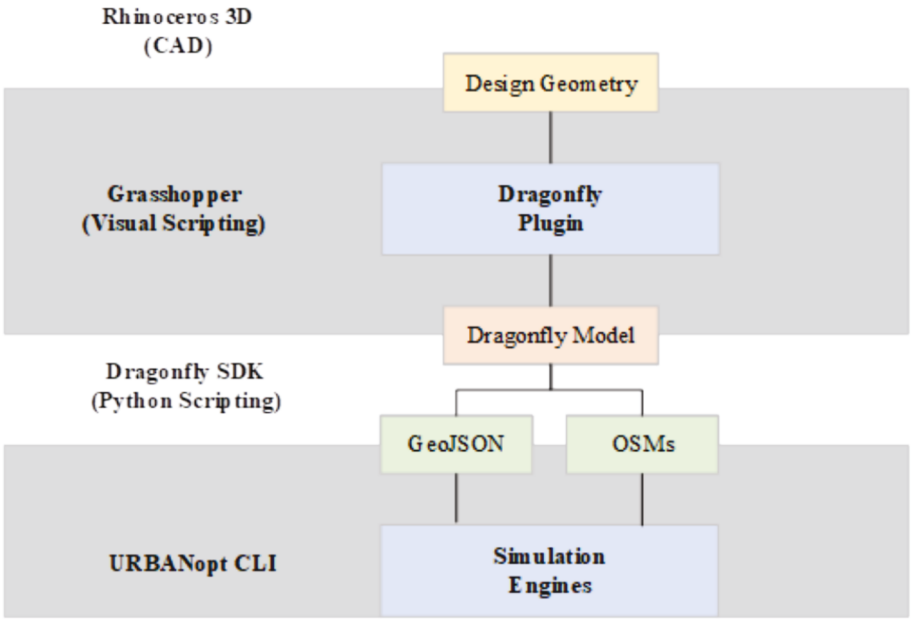

Fig. 6. Workflow schema for URBANOpt simulation.

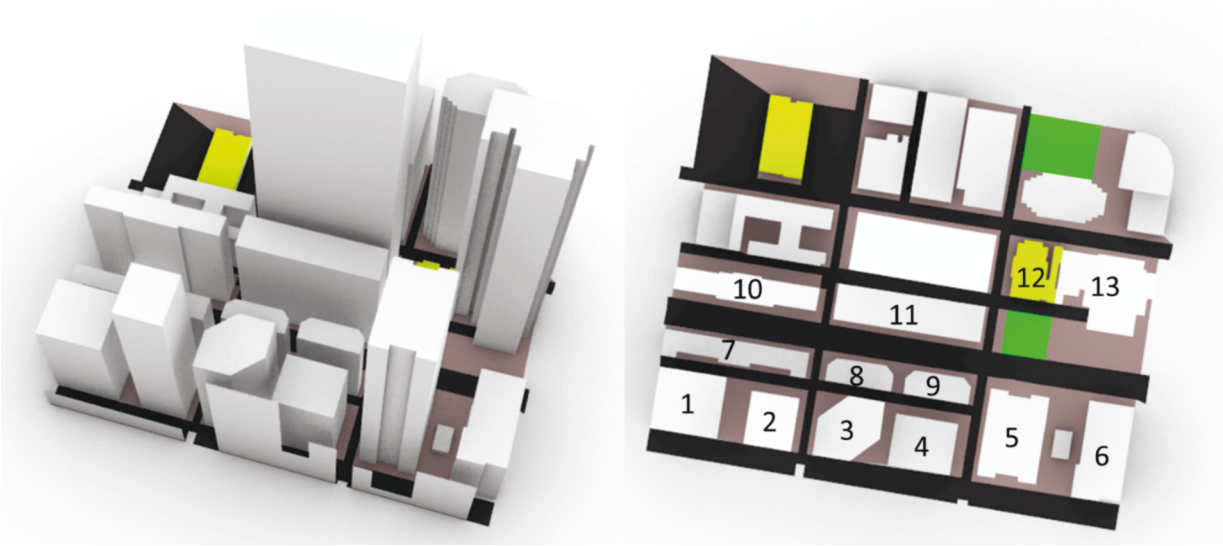

Fig. 7. Focused Urban Area for District-Level Building Energy Use Analysis.

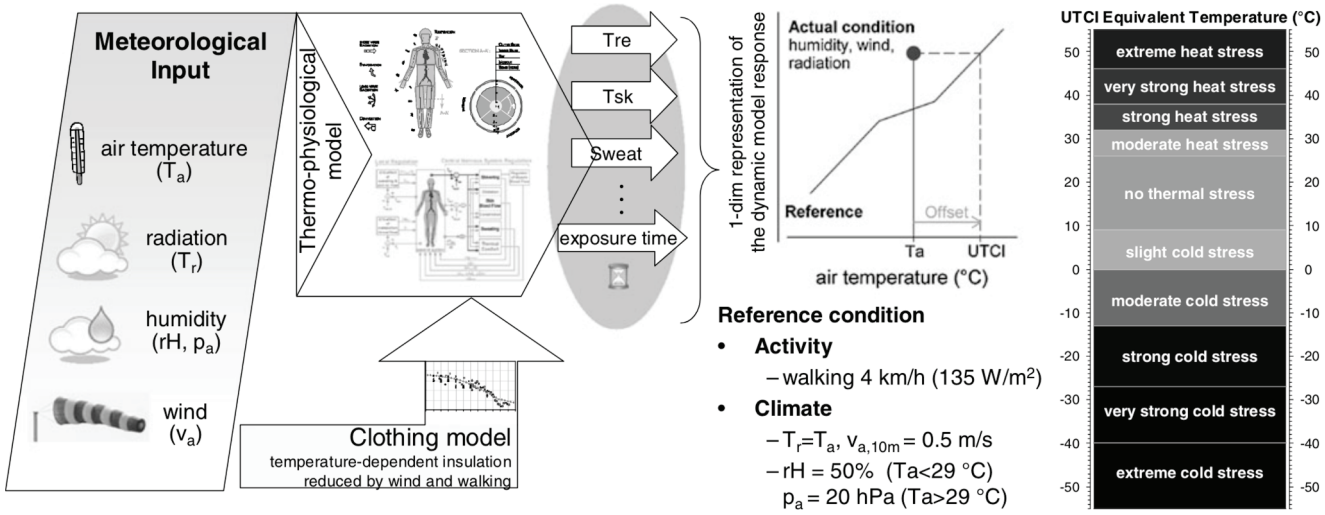

Fig. 8. Concept of UTCI derived as equivalent temperature from the dynamic multivariate response of the thermophysiological UTCI-Fiala model (Fiala et al., 2011), which was coupled with a clothing model (Havenith et al., 2011).

involve dry-bulb air temperature (T_a), mean radiant temperature (T_{mrt}), water vapor pressure (P_a) or relative humidity (RH), and wind speed (V_a) (at the elevation of 10 m). This can be written in the mathematical equation as:

$$UTCI(T_a, T_{mrt}, V_a, P_a) = T_a + Offset(T_a, T_{mrt}, V_a, P_a)$$

$$UTCI = 3.21 + (0.872 \cdot T_a) + (0.2459 \cdot T_{mrt}) - (2.5078 \cdot V_a) - (0.0176 \cdot RH)(^{\circ}\mathrm{C}) \quad (3)$$

Non-meteorological parameters were set as default: with a body standing/walking (with a metabolic rate around 2.4 met), the solar horizontal angle relative to the front of a person (SHARP) was 135 degrees, absorptivity was 0.7 (for average skin and medium clothing) and emissivity was 0.95. The basic logic flow of producing the UTCI index using Ladybug tools, as shown in Fig. 9, involves three key steps:

- Mean radiant temperature (MRT) at each sensor was divided into two parts: longwave MRT and shortwave MRT. Longwave MRT contains the radiant exchange between the human body, sky, and surrounding building surfaces, while shortwave MRT mainly considers the radiant exchange between the human body and direct sunlight.
- The air temperature (T_a) of the studied area was adjusted by considering the Urban Heat Island (UHI) effect. Normally, the air temperature of an urban area will be a few degrees higher than a rural area (where EPW files are recorded).
- Air velocity (V_a) at each sensor point was produced by coupling CFD analysis with EPW wind speed and direction.

Longwave MRT was calculated by multiplying the view factors of each sensor with the sky temperature and surrounding buildings' surface temperatures. This step was done by utilizing the outside surface heat balance equation inside EnergyPlus. Longwave MRT, however, was expected not to have a great influence on UTCI when surface reflectance changed, as EPW sky temperature was fixed and building surface temperature would not change much considering a relatively fixed façade solar absorptance. Shortwave MRT compensates for longwave MRT by considering the effect of shortwave solar radiation on human thermal comfort, it can be expressed using the following equations:

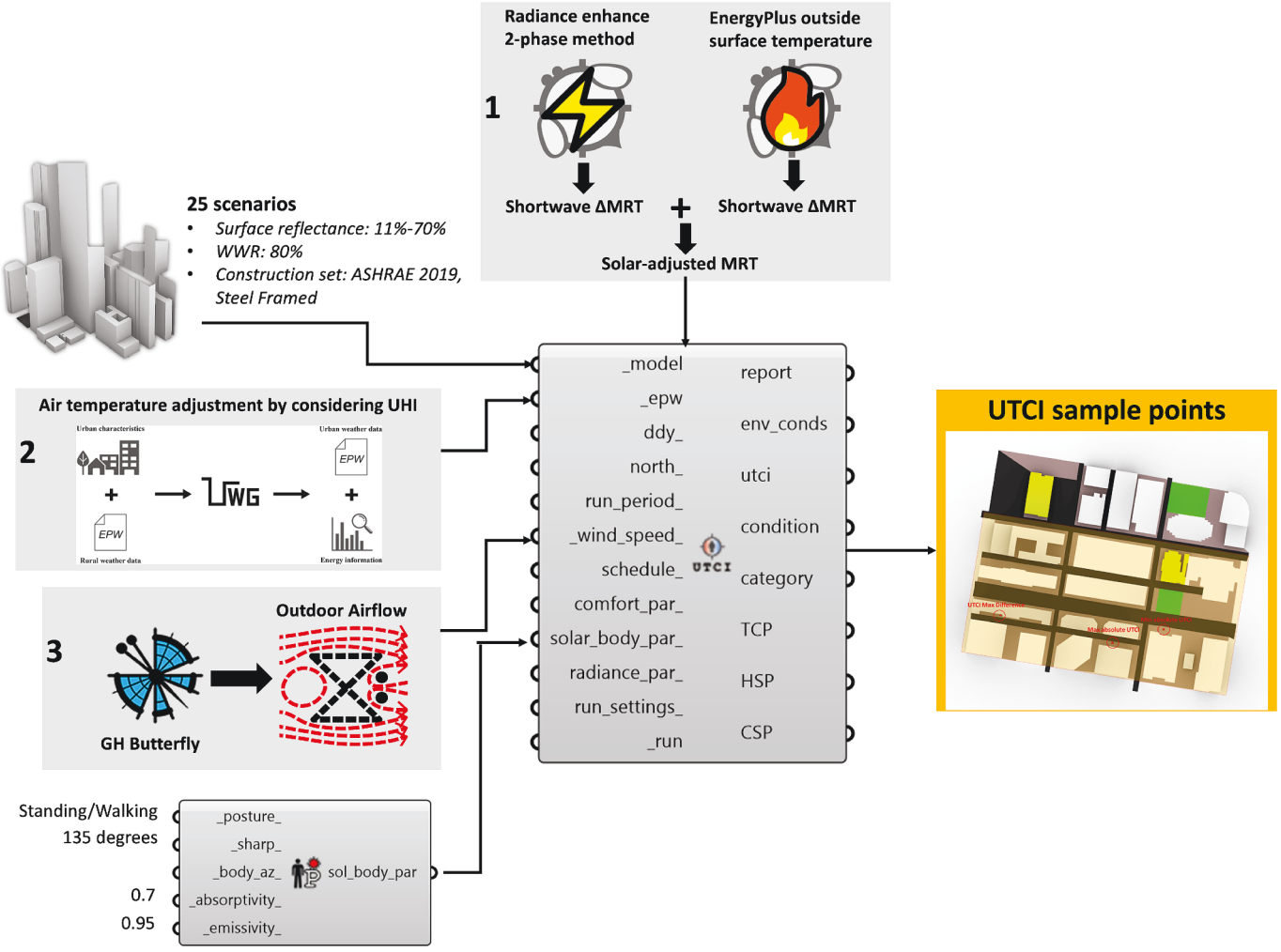

Fig. 9. Workflow Schema of UTCI Analysis in GH, Honeybee Plug-in.

$$MRT_{LW} = \left(\sum_{i=1}^{N} F_i \cdot T_i^4\right)^{1/4} - 273.15(^{\circ}\mathrm{C}) \tag{4}$$

$$T_{sky} = \sqrt[4]{\frac{L_{sky}}{0.95 \cdot \sigma}} - 273.15(^{\circ}\mathrm{C}) \tag{5}$$

$$MRT = MRT_{LW} \cdot \left(1 - \frac{F_{\mathrm{sky}}}{2}\right) + T_{sky} \cdot \left(\frac{F_{\mathrm{sky}}}{2}\right) + \frac{ERF}{h_r \cdot f_{eff}}(^{\circ}\mathrm{C}) \tag{6}$$

$$ERF = f_{eff} h_r (MRT - T_a) \tag{7}$$

$$ERF_{solar} = (0.5 f_{eff} f_{svv} (I_{diff} + I_{TH} R_{floor}) + \frac{A_p f_{bes} I_{dir}}{A_D}) T_{sol} (\frac{\alpha_{SW}}{\alpha_{LW}}) \tag{8}$$

where ERF is an effective radiant field (used to describe the additional longwave radiation energy at the body surface when surrounding surface temperatures are different from the air temperature), ERF_{solar} is effective radiant field solar component (which is added to longwave ERF in Eq. (7) to determine solar-adjust MRT, i.e., ΔMRT, by using Eq. (6)), f_{eff} is the fraction of the body surface exposed to radiation from the environment, f_{svv} is the faction of sky view, f_{bes} is the faction of the body exposed to sunlight, A_p is the projected area of a standard person exposed to direct beam sunlight, A_D is the DuBois surface area of the person, h_r is the radiation heat transfer coefficient, I_{diff}, I_{dir}, and I_{TH} are diffuse, direct and global horizontal solar irradiance [48]. By using a Radiance-based enhanced 2-phase method, ground solar irradiance can be produced by tracing a sun-ray from each sensor to the solar position. The shortwave radiant exchange between the human body and the sun was then converted into shortwave MRT by using the SolarCal model proposed by *Aren et al.* [48].

Air temperature within dense urban areas was expected to be a few degrees higher than that in non-urban areas (where most TMY3 weather stations are located) because of the Urban Heat Island (UHI) effect. By taking the urban environment and anthropogenic activities into consideration, more accurate city-center air temperature can be simulated in the modeling process, based on the existing TMY3 weather files. In this study, the Urban Weather Generator (UWG) developed by Bruno *et al.* [49–51] was used to predict the adjusted air temperature within the urban canopy. UWG is a physics-based microclimate simulation tool, designed to simulate the effects of the urban environment on local weather conditions and to assess the energy performance of buildings in urban areas. It also considers the anthropogenic energy interactions within the urban environment, such as heat released from building operation, and traffic vehicles, by embedding a building energy model in the scheme and prescribing a traffic-generated heat (which normally remains at 8–15 W/m^2 in many cities [49]) in canyon energy balance. UWG could process the EPW data and generate the simulated urban weather data, as shown in Fig. 10. The newly generated urban weather data can then replace the original weather data and be used in the following UTCI simulations. In this study, a GH Dragonfly plug-in UWG was used to simulate the adjusted urban weather file by modifying building UWG properties (more specifically, SHGC, which is used to

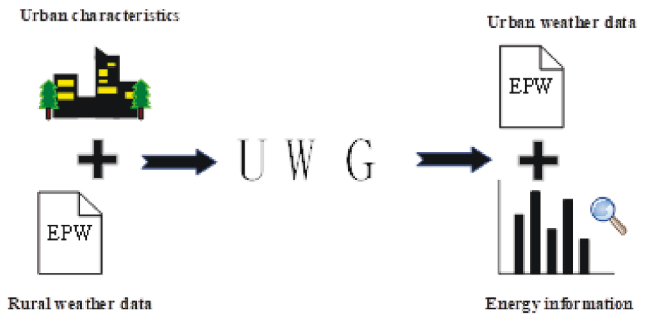

Fig. 10. General workflow of the UWG.

evaluate the amount of solar heat reflected back to the street canyon) [52].

Wind velocity is another important factor that could influence UTCI results. Therefore, a CFD analysis for this city-scaled model is necessary. By placing the 'probes' at each sensor and setting the wind scenarios for each timestep, the time-series air velocity can be solved for every sensing point within the analysis period. To accomplish this, the GH Butterfly plug-in (OpenFOAM embedded) was used, and the Steady Reynolds-Averaged Navier Stokes (RANS) approach was utilized to solve the governing equation of fluid motion.

All 25 building external-wall scenarios were simulated and compared in this UTCI analysis. The other information such as the basic construction set was consistent with previous simulations. Window-Wall Ratio, however, was set as 80 % universally. Based on the previous ground solar irradiance – building surface reflectance interaction, this analysis will focus on the lower half of the urban model, as shown in the yellow area of Fig. 11. The grid size was set as 3 m by 3 m, and 1.4 m above ground [53], with both quadrilateral and triangular meshing (4448 sensors in total). The simulation period was set the same as ground solar irradiance analysis, from 12:00 PM to 17:00 PM, on Aug 18th. For consistent and representative comparisons of the façade reflectance's impacts, we particularly selected three specific points based on the simulated UTCI results (shown in Fig. 11). Notably, these points were representative, meaning that there were other spots in the study area with identical or similar magnitudes of UTCI variations caused by different facades. In addition to these extreme sampling points, the average UTCI values in the study area were also calculated and involved in the correlation analysis and comparisons. Lastly, the percentage area of the simulated urban domain that exceeds 38 °C strong heat stress threshold was also compared and reported to compare the influence of building surface reflectance on urban-scale thermal comfort level.

Fig. 11. Sampling points in the study area for UTCI comparison in 25 scenarios.

3.6. Validation

In our integrated computational methodology, there are two centric computed parameters: the UWG weather conversion to local environments and the reflected global solar radiations in the urban canyon. These two variables are the foundational elements for further physics-based computations, such as MRT, and subsequent UTCI computations. To validate the accuracy of our methodology in computing these parameters, we drew upon the empirical investigations encapsulated in the research on the interplay between reflective materials and urban canyon albedo by *Salvati et al.* [3]. Their research offers a repository of exhaustive field data concerning urban canyon reflective radiation and ambient thermal conditions, accompanied by meticulously crafted digital representations incorporating refined envelope configurations and urban textures. In particular, we used our computational methodology to construct all urban canyon models described by Salvati *et al.*, and then computed and compared local ambient outdoor air temperature and reflected solar radiation in the urban canyon against the empirical measurements reported in their studies [3,54]. The error percentage between the measured and simulated parameters was reported.

3.7. Multi-objective optimization

In multi-objective optimization problems, the main task of the algorithm is to simultaneously minimize or maximize the objective function. Therefore, all objective functions are defined as a vector, as shown in the following equation:

$$\max Xor\min y = (f_1(x), f_2(x), \cdots, f_n(x))$$

$$x = (x_1, x_2, \cdots, x_m) \in X$$

$$y_1, y_2, \cdots, y_{PF} \in Y \quad (9)$$

The objectives of this study are to minimize both district-level energy use intensity (including heating, cooling, and lighting), UTCI, and Area of $UTCI_{>38}$, with glazed façade systems' properties (such as R_{fsol}, SHGC, and T_{vis}) as decision variables. Among all the decision variables, UTCI is mainly dependent on R_{fsol}, while $EUI_{heating,\ cooling,\ lighting}$ are mainly dependent on SHGC, U-factor, and T_{vis}. Therefore, the objective function of this study can be defined as:

$$\min y = \left(EUI(SHGC, U-factor, T_{vis}), UTCI(R_{fsol}), AreaofUTCI_{>38}(R_{fsol})\right) \quad (10)$$

4. Results

4.1. Validation of simulated environmental data against empirical measurements

Fig. 12 (left) displays a comparison between simulated and measured reflected solar radiation for a point located in the urban canyon over the course of the selected day. The close alignment of the two curves suggests that the simulation model accurately reflects actual conditions, with a high degree of correlation (Pearson correlation of 0.99, P value $<$ 0.01). This indicates a strong relationship between the simulated and measured values, confirming the model's reliability. Despite this strong correlation, there is an observed error percentage of 8.6 %, which, while noteworthy, still falls within an acceptable range for such simulations. The relatively larger errors during the afternoon may be attributed to the significant fluctuations in actual solar conditions. As for outdoor air temperature inside the urban center, Fig. 12 (right) presents the comparison between the simulated air temperature data against actual measurements for the selected points over a day. With an error percentage of only 3.8 %, the simulation closely matches the measured temperatures. The data follows a typical diurnal pattern, with both simulation and measurement reflecting the rise in temperature during

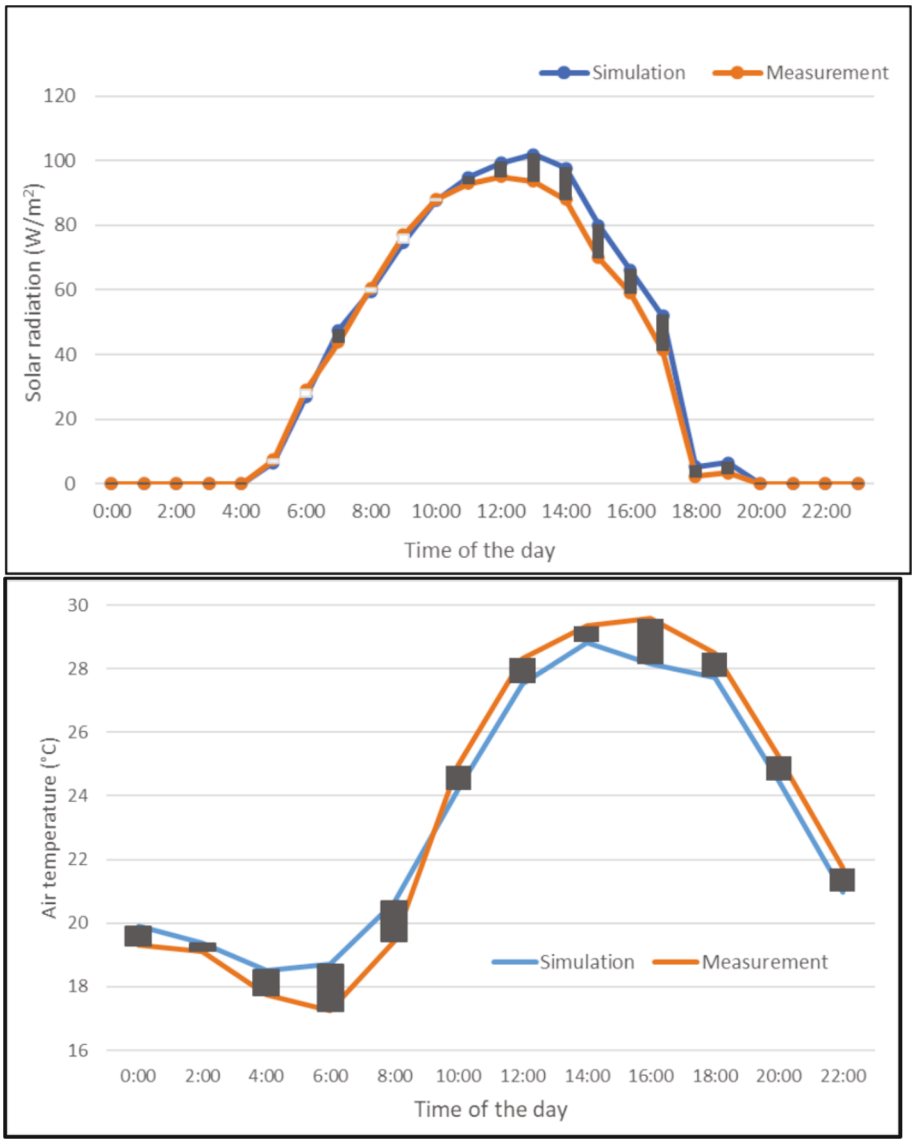

Fig. 12. Simulation and measurement comparison based on Salvati et al.'s study [3].

the day and a decrease at night. The peak temperatures occur around the same time for both sets of data, indicating that the simulation is well-tuned to the measured environment. Overall, the validation results suggest that the proposed computational method is reliable and suitable for further analysis and predictive modeling in studies of reflected solar radiation in urban environments.

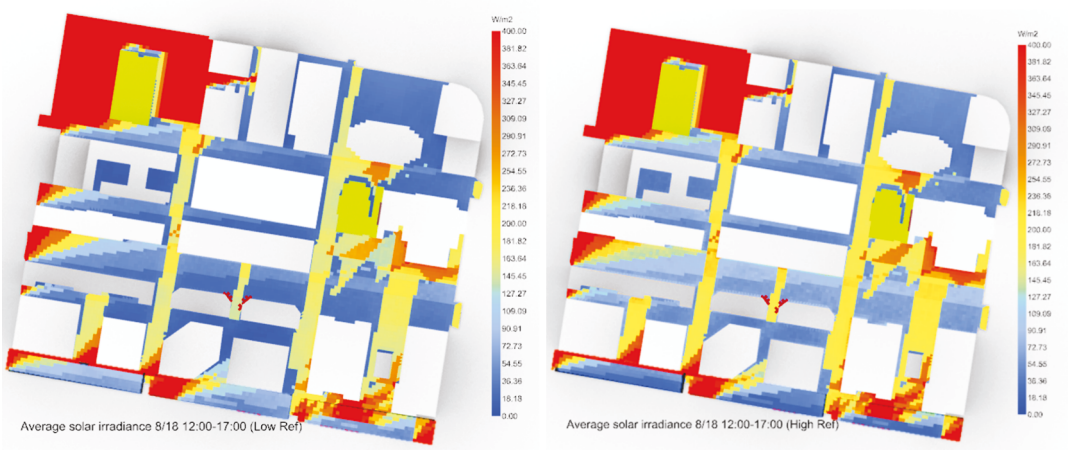

Fig. 13. Average ground solar irradiation at 12:00–17:00 PM, 8/18 (Left: Low building façade reflectance; Right: High building façade reflectance).

4.2. Façade reflectance impacts on outdoor ground solar irradiance

Based on the above-illustrated radiance-based simulation methods, we obtained a series of solar irradiation (for a period of time) and irradiance (average solar power) results on the defined grids. Fig. 13 showcases a comparison of average solar irradiation on the ground within the selected urban block from noon to 5 PM on August 18th, under two extremely different conditions of building facade reflectivity. It presents a more muted distribution of solar irradiance with cooler tones dominating the scene on the left (Low R_{sol}: low solar reflectance, 0.11), indicating average lower levels of solar energy reaching the ground. On the right (High R_{sol}: high solar reflectance, 0.70), high reflectance facades result in a brighter and warmer color palette, signifying a substantial increase in solar radiation impacting the ground. The average ground solar radiation across the whole study area increased by 27.54 W/m^2 (or 16.9 %) from the low to high solar reflectance scenario. The highest solar radiation change is approximately 95.15 W/m^2, which was almost 3.4 times higher than the solar radiation in the low R_{sol} scenario. This comparison starkly illustrates how the reflectivity of a building's facade can dramatically alter the amount of solar energy that is either absorbed or reflected back into the urban environment. While the overall patterns remain consistent with the cumulative analysis, the average irradiance highlights the immediate solar loading, which can have significant implications for the thermal comfort of pedestrians and nearby buildings.

4.3. Façade reflectance impacts on district-level energy use intensity

Fig. 14 illustrates the relationship between the district-level Energy Use Intensity (EUI) and the solar reflectance of building façades. EUI is measured in kilowatt-hours per square meter (kWh/m^2), representing the energy consumed by the district's buildings. As the solar reflectance of the façade materials increases (x-axis), the EUI for cooling (orange area) shows a significant decrease. This indicates that higher solar reflectance in building materials reduces the solar heat gain within buildings, thereby lowering the demand for cooling energy. This is aligned with our initial expectation about using solar reflective surface retrofits for energy savings. On the other hand, the EUI for heating (blue area) displays a slight increase with higher reflectance. This could be due to the reduced passive solar heating in cooler months, necessitating more active heating, while such increases are still smaller compared with the cooling energy savings due to the façade's solar reflectance increase. In particular, with the increase of solar reflectance of glazed facades, the cooling energy reduction achieved about 26.4 kWh/m^2, while the increase in heating energy use was only about 12.4 kWh/m^2.

The nuanced variations in heating energy use across different levels of solar reflectance can be attributed to the interplay between the solar heat gains and the U-factor, which measures the rate of heat transfer through a building element. At a solar reflectance of around 0.25, there was an optimal balance where the building absorbed enough solar energy to minimize heating requirements without excessive heat loss. As solar reflectance decreased to 0.1, the façade absorbed more solar energy, but this also led to increased heat loss due to higher thermal conductance, especially in the absence of low-emissivity coatings, which can exacerbate the heating energy demand. Conversely, as reflectance increased to 0.7, while there was less solar heat gain, the U-factor may increase if the façade system lacks low-e coatings, leading to greater heat loss and hence increased heating energy use. In simpler terms, high reflectance without appropriate thermal insulation can result in more heat escaping from the building, which cannot be compensated for by solar heat gains, particularly in cooler periods. In contrast, the cooling energy showed a more consistent trend; as solar reflectance increased, the U-factor tended to decrease up to a certain point. This reduction lowered both the radiative and conductive heat gains through the building's façade, leading to a substantial reduction in cooling energy requirements. The facade's increased reflectivity effectively repels solar radiation, which helps to keep the interior of the building cooler and reduces the reliance on air conditioning systems.

The EUI for lighting, indicated by the grey area in the graph, does not show significant fluctuations with changes in solar reflectance when viewed in the context of total energy usage. However, when examining the details in Fig. 15, it is observed that there is a subtle but noticeable increase in artificial indoor lighting energy use as the solar reflectance of the façade rises, particularly when the solar reflectance exceeds 0.5. This pattern suggests that higher reflectivity of façade materials can lead to a decrease in natural daylight availability inside the building, known as the visible transmittance (T_{vis}), thereby necessitating more artificial lighting. To summarize, the overall EUI is observed to significantly decrease, from 140.8 to 109.8 kWh/m^2 (~22 %) with increasing solar reflectivity from 0.11 to 0.7—largely due to lowered building cooling energy demands. However, solar-reflective façades still increase energy consumption for heating and lighting, particularly in regions where the balance between solar gain and loss is critical to energy efficiency.

4.4. Façade reflectance impacts on UTCI

Employing the methodology outlined in Section 3.5, we captured the distribution of the UTCI across a designated urban analysis grid. Each

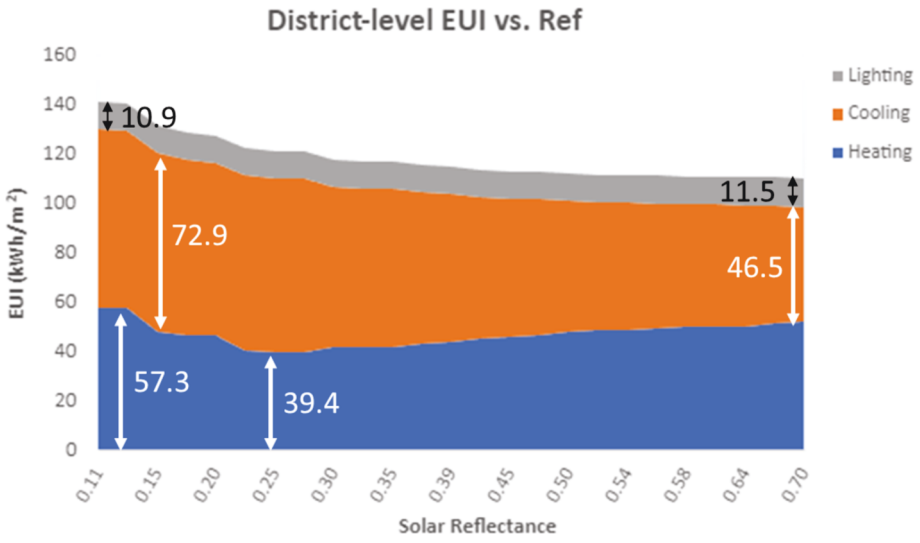

Fig. 14. Correlation between district-level EUI and building façade solar reflectance.

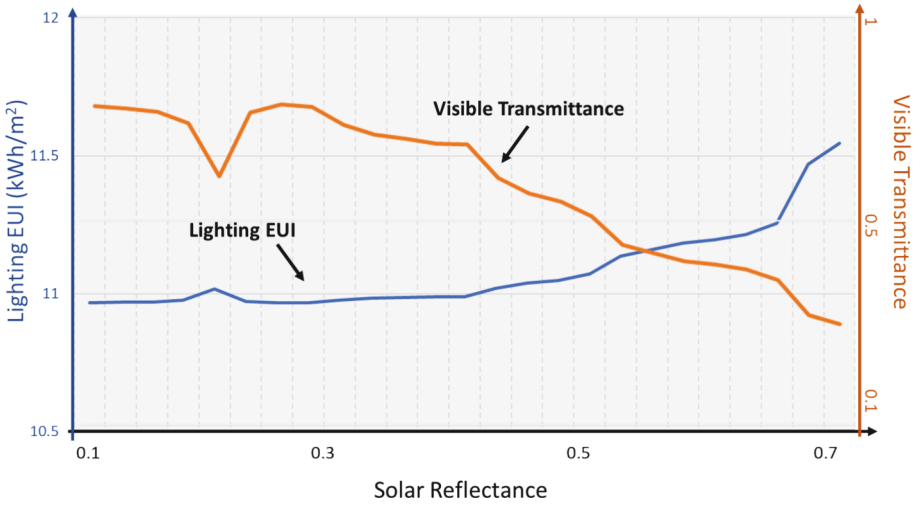

Fig. 15. Detailed view of lighting EUI, $T_{vis,}$ and building façade solar reflectance.

grid point reflects a time-averaged UTCI temperature, with simulations purposefully conducted during periods of elevated solar radiation and ambient temperatures to assess the possible effects during heatwave conditions. The simulation results depicted in Fig. 16 provide a vivid comparison of the UTCI distribution in the selected dense urban area, influenced by the solar reflectance (0.11 left vs. 0.70 right) of building facades. The simulation results across two scenarios with different solar reflectance of facades shed light on the thermal conditions humans might experience in similar urban settings.

Common to both distribution images is the depiction of UTCI variation across an urban setting, highlighting the critical influence of high-rise building orientation on outdoor local thermal comfort. The orientation affects how buildings receive and trap direct solar radiation, with south-north alignments particularly susceptible to capturing intense solar rays, thereby increasing local UTCI values. Upon comparing the two distributions, distinct differences emerge as a result of varying facade solar reflectance. In the scenario with low solar reflectance (0.11), the UTCI suggests areas of moderate thermal stress. This level of stress is generally considered acceptable and does not pose significant health risks. It may even be perceived as comfortable in comparison to higher stress levels, especially during warmer periods when some heat is tolerable. Conversely, the high solar reflectance scenario (0.7) shows elevated UTCI values, entering ranges that indicate extreme heat stress. Such conditions can lead to strong thermal discomfort, heat exhaustion, or even other heat-related health issues, especially for vulnerable populations or during physical activity outdoor. The average UTCI increment across the overall study area is 1.28 °C, when comparing the low solar reflectance (0.11) case with the high reflectance (0.70) case, indicating the overall negative impact of high solar reflective façade on outdoor thermal conditions during hot summer days. The areas that show the greatest difference in UTCI values, highlighted in the simulation map, are of particular concern as they exceed a 3 °C difference, indicating a substantial increase in heat stress due to the facade's higher solar reflectance.

With the same simulation methods for the selected period, we obtained the UTCI distributions for all different 25 façade models. Fig. 17 shows a correlation between the solar reflectance of glazed facades and the percentage area experiencing high UTCI values exceeding 38 °C, indicative of strong and even extreme heat stress. Initially, as the solar reflectance values increase from 0.11 to 0.25, the percentage area of high UTCI values rises only marginally, suggesting a relatively stable relationship between facade reflectivity and outdoor heat stress. However, beyond a solar reflectance of 0.25, a more pronounced increasing trend is observed. The area experiencing high UTCI values begins to escalate more noticeably with each incremental rise in solar reflectance. This upward trend continues consistently as the solar reflectance values

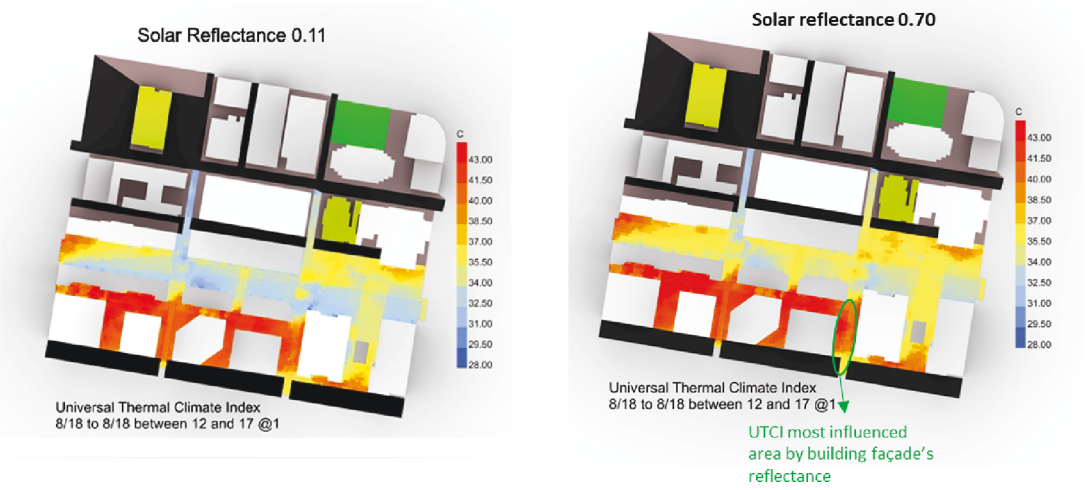

Fig. 16. UTCI Thermal map low and high reflectance.

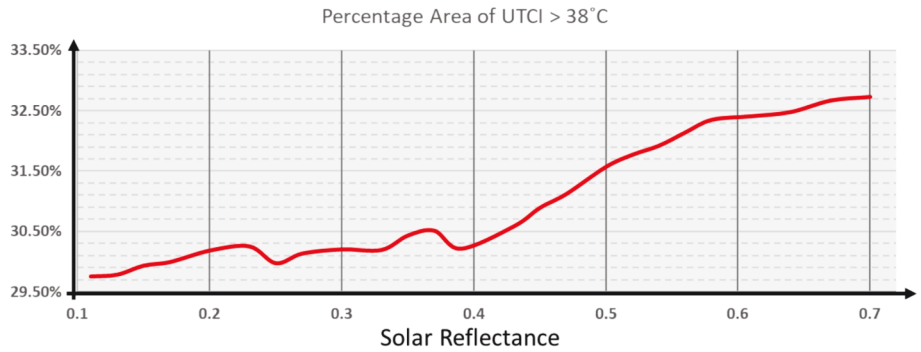

Fig. 17. Percentage area of UTCI > 38 °C (suggesting very strong heat stress).

reach 0.70, with the percentage area of high UTCI values peaking at almost 33 %. While the data indicates a seemingly modest 4 % increase in the area experiencing extreme heat stress when transitioning from low to high solar reflectance facades, the actual impact on urban life should not be underestimated. In this case study context, such 4 % represent about 1,200 m^2 of urban areas, which may often serve as open spaces and hubs where people congregate for leisure, transit, and other daily routines. Therefore, even a small increase in areas with high UTCI values could significantly affect outdoor comfort and public health. This, again, suggests that higher solar reflectance in building façade materials, while potentially reducing heat gains by the structures themselves, may contribute to increased heat stress in the surrounding environment, exacerbating conditions that lead to thermal discomfort and potential health risks for individuals in outdoor urban spaces.

The regression analysis provided in Fig. 18 illustrates the general linear relationship between the solar reflectance of facades and the UTCI values, including the average of the overall study area, the value at the maximum difference point, the value at the maximum point, and the value at the minimum point. In general, as the solar reflectance (R_{sol}) increases, all four UTCI values also increase but with different magnitudes. From the perspective of average UTCI, an increase in reflectance negatively impacts the UHI, though some areas may respond more sensitively to variations in building facades, warranting further investigation and treatment. From the listed regression functions in the plot, it is evident that the "Max difference UTCI" has the highest coefficient or slope, indicating the strongest impact by the R_{sol} variation, while the "Min UTCI" presents a relatively weak linear relationship with a lower slope and more scattered data points. This suggests that although the minimum UTCI values rise with increased reflectance, but not as steeply as the UTCI values extracted in other points or areas. This is understandable since the solar reflectance of facades did not uniformly influence the outdoor thermal environments.

In addition to the UTCI value analysis, we also extracted the MRT values (key output parameters influenced by solar radiation and solar reflection and determined the UTCI values). Fig. 19 reveals that the underlying reasons for the rise in UTCI values due to the high solar reflectance of building facades are deeply rooted in the role of Mean Radiant Temperature (MRT), particularly shortwave MRT. The regression analyses across these two sets of plots exhibit a direct and clear positive correlation—higher building facade reflectivity was associated with an increase in MRT, which quantifies the radiative heat experienced by individuals. The top overall MRT plot demonstrates that with higher reflectance, there is a substantial rise in both the maximum MRT and its differential, potentially intensifying thermal stress in dense urban areas, and adversely affecting human comfort. The bottom shortwave MRT plot further highlights this trend, showcasing an even more pronounced positive correlation (higher slope in the plot or greater coefficient in the regression function) for shortwave MRT. This implies that surfaces with higher solar reflectance are likely to amplify shortwave radiation locally, thus increasing the MRT and possibly aggravating the urban heat island phenomenon. The analysis suggests that longwave MRT had a negligible influence in this specific study, as the glazed facades under investigation exhibited minimal variation in their absorption characteristics, making minor contributions to changes in absorbed and re-radiated solar energy. Collectively, these insights underscore the critical need to factor in solar reflectance in urban planning to balance indoor cooling benefits against the risk of elevated outdoor thermal stress, thereby safeguarding outdoor thermal comfort.

4.5. *Optimization of façade's solar reflectance*

From the above district-level EUI and UTCI results, it can be concluded that the most sensitive objectives that can be influenced by building façade properties were: cooling EUI and outdoor UTCI at maximum difference points. Therefore, the Pareto Front was plotted for two different objectives: Cooling EUI vs. UTCI at the maximum differential point, along with Total EUI vs. UTCI at the maximum differential point. The Pareto Front graph in Fig. 20 depicts in the image illustrates a trade-off between the UTCI, representing outdoor thermal comfort, and Cooling EUI, which measures the efficiency of energy use for cooling buildings. The blue data points represent various combinations of building façade properties and their resulting UTCI and Cooling EUI values, while the red line represents the Pareto Front, showcasing the most efficient combinations where any improvement in one objective

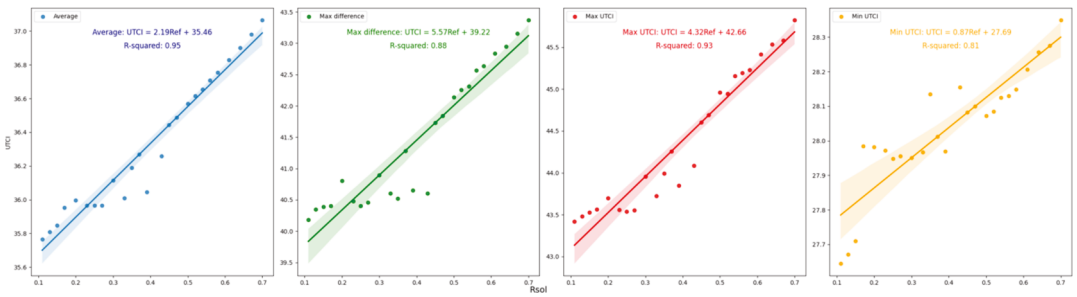

Fig. 18. Linear regression analysis for correlation between building façade reflectance and UTCI values.

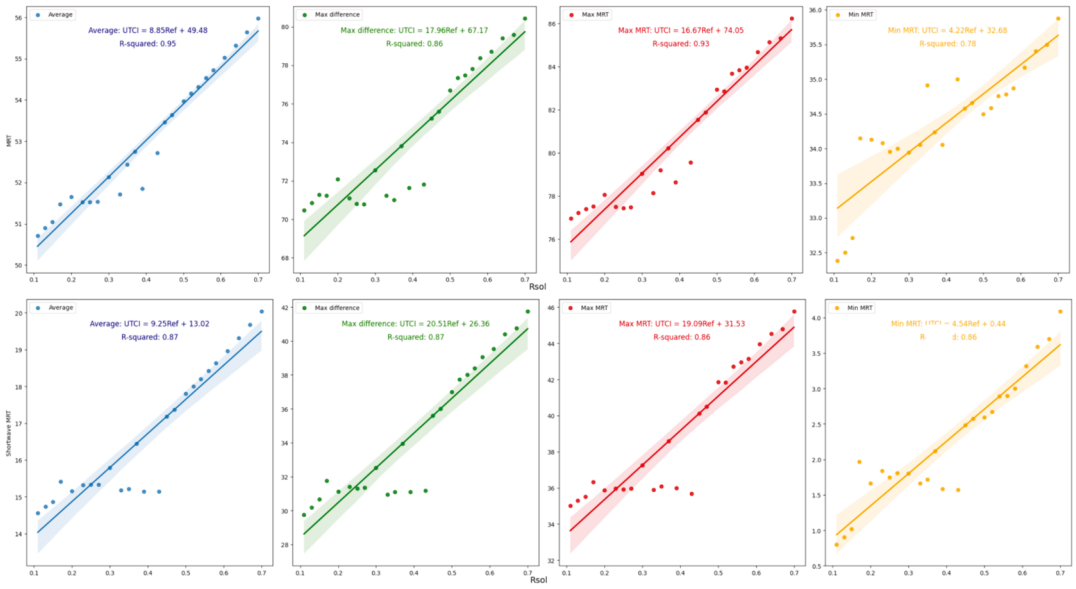

Fig. 19. Linear regression analysis for correlation between building façade reflectance MRT at sampling points (Top: Overall MRT; Bottom: Shortwave MRT).

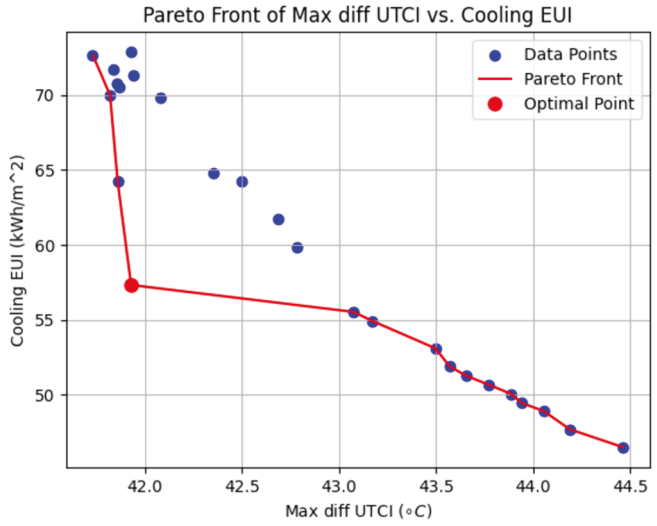

Fig. 20. Pareto Front for UTCI vs. Cooling EUI.

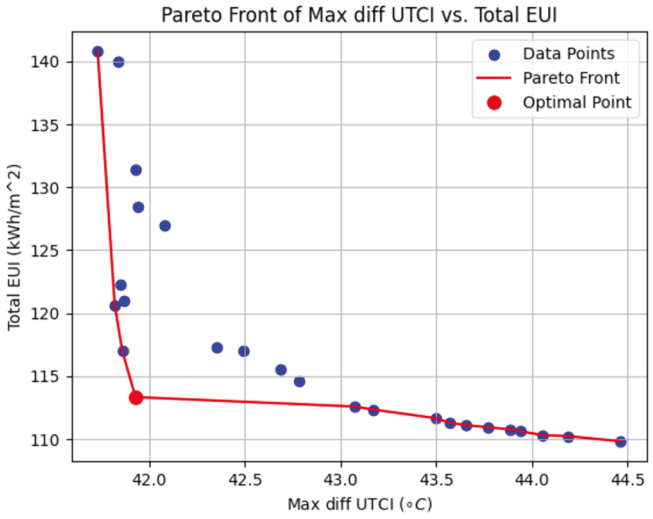

Fig. 21. Pareto Front for UTCI vs. Total EUI.

would lead to a deterioration in the other. The plot shows that the optimal point on this front is highlighted as an outlier, with a UTCI value of 41.93 °C which is very close to the minimum UTCI value of all model simulation results (which is 41.73 °C). It also brings the acceptable cooling EUI, 57.3 kWh/m^2, which, while not the absolute lowest (i.e., 46.5 kWh/m^2), represents a balanced compromise between energy efficiency and thermal comfort. The façade properties at this optimal point suggest a visible transmittance (Tvis) of 0.60 and a Solar Heat Gain Coefficient (SHGC) of 0.35, indicating a moderate level of solar radiation allowed through the glass. The U-factor at this point is 1.35 W/m^2·K, pointing to a lower façade's thermal conductance. From the plot, it can be also observed that the recommended solar reflectance range of 0.30–0.50 balances the need to avoid extreme UTCI values and excessive energy use for cooling, making it a crucial factor in façade design for urban areas where both energy efficiency and thermal comfort are significant concerns.

To ensure the optimal search by the Pareto front analysis between the cooling EUI and UTCI, additional optimization work about the trade-off between the total EUI and UTCI was also conducted, as shown in Fig. 21. The illustration in the energy impact section explains that there was a minor trade-off issue between the cooling, heating, and lighting energy use due to the change of solar reflectance of glazed facades. However, the Pareto Front depicted in Fig. 21 underscores a similar trade-off to the Cooling EUI versus UTCI. The same optimal point and the same facade reflectance range recommendation of 0.30–0.50 emerge again as critical factors, advocating for facades that effectively balance energy and comfort requirements. This additional optimization validates the earlier findings, reinforcing the need for integrated facade design strategies that simultaneously address energy efficiency and urban livability.

5. Conclusion

5.1. Nexus of sustainability and thermal resilience to extreme weather

Retrofitting with high solar-reflective surfaces, as seen in this study, is a specific but representative example where sustainability efforts improve internal thermal comfort and resilience. However, strategies focused solely on individual buildings may not always yield positive outcomes for broader urban thermal resilience. This dynamic

necessitates a comprehensive, interdisciplinary approach to understanding the effects of sustainable features at various scales – from individual buildings to entire urban and rural regions. Resilience and sustainability are not static phenomena that can be accelerated and amplified by processes of global, local, and social change. Developing such a multiscale thermal resilience assessment framework requires collaboration across architectural engineering, sociology, urban planning, and other fields. This framework should integrate both physical and social context variables and span multiple levels, including individual occupants, households, buildings, and communities. By using a combination of experiments, simulations, and surveys, such research efforts can uncover how thermal resilience is influenced by specific physical, social, and urban contexts during the transition to sustainable practices. The resulting framework, based on these insights, will provide a means to balance sustainability transitions and resilience to climate-related challenges across urban and rural areas. Such a holistic approach is vital for preparing and responding effectively to extreme temperature events, ensuring both sustainable development and enhanced resilience.

5.2. Remarks of findings

This research offers a comprehensive examination of how solar reflectance in building facades influences urban microclimates and indoor energy efficiency. Our analysis has demonstrated that higher facade reflectance reduces the building's EUI but can lead to increased outdoor UTCI values, implying heightened outdoor heat stress. Specifically, an increase in facade solar reflectance led to a cooling energy saving of approximately 26.4 kWh/m^2, while the heating and lighting EUI experienced a modest and slight rise, respectively. Such collective effects still enable the high solar reflective façade to achieve up to 22 % building energy savings. In contrast, the increase in facade reflectance correlates with a rise in UTCI values, suggesting greater heat stress with about a 4 % increase in the area experiencing extreme heat stress when transitioning from low to high solar reflectance glazed façades. Such impacts on UTCI are particularly greater when reflectance exceeds 0.25. The nuanced UTCI metric analyses revealed that the shortwave MRT played the most important role in influencing the outdoor thermal environment because of the solar reflective façade applications. Therefore, the research underscores the complexity of the relationship between building facade reflectance, individual building energy savings, and urban thermal comfort, with higher reflectance potentially exacerbating heat stress in urban canyons. Further analysis through optimization models indicated a delicate balance between indoor energy efficiency and outdoor thermal comfort. The Pareto optimization front showed that a facade with a reflectance of 0.43 yields an optimal compromise, with an acceptable UTCI and reasonable EUI savings. Beyond this optimal point, higher reflectance begins to significantly elevate UTCI without substantial gains in cooling energy efficiency.

5.3. Future works

This research has advanced our understanding of facade reflectance on urban microclimates and building energy efficiency, yet it identifies several avenues for future research inquiries. The 2-phase Radiance method employed here may not fully capture the complexities of solar irradiance within urban settings, necessitating more sophisticated modeling techniques. The computational intensity of simulating extensive urban areas has limited the sample size, geometrical elements, and outdoor human postures and behaviors, possibly affecting the robustness of statistical conclusions. Furthermore, the exclusive focus on the optical properties of glazed facades has overlooked other urban form factors, such as canyon ratios and facade configurations, and their interactions with specific solar paths/positions, which could significantly influence energy consumption and outdoor thermal comfort. In light of these insights, future research should pivot towards dynamic facade systems capable of responding to changing solar exposures and incorporating green infrastructure to bolster thermal regulation. Thirdly, it is worth exploring the effects of different urban canyon types and characteristics on the UTCI variations caused by different façade design parameters. This would require a large number of simulations and numerical analyses. Embracing a data-driven approach for such studies holds considerable promise for sustainable urban development, balancing indoor energy efficiency and thermal comfort with the imperative of managing outdoor thermal effects. Lastly, from the perspective of glazed façade material design and engineering, *retro*-reflective technologies present a promising direction, though they may encounter difficulties due to the requirements for high visible transmittance and view quality. Future research should aim to develop transparent films that combine *retro*-reflection with spectral selectivity, focusing on the solar infrared while maintaining clarity in the visible range. This direction could significantly advance the application of *retro*-reflective technologies in glazed façades, addressing current limitations and enhancing their effectiveness.

CRediT authorship contribution statement

Chenshun Chen: Writing – original draft, Visualization, Validation, Investigation, Formal analysis. **Julian Wang:** Writing – review & editing, Supervision, Project administration, Methodology, Conceptualization. **Huijin Zhang:** Software, Formal analysis, Data curation. **Xinyue Xu:** Software, Investigation, Formal analysis. **Laura Elizabeth Hinkle:** Software, Investigation, Data curation. **Xiao Chao:** Validation, Methodology. **Qian Shi:** Supervision, Resources, Funding acquisition.

Declaration of competing interest

The authors declare that they have no known competing financial interests or personal relationships that could have appeared to influence the work reported in this paper.

Acknowledgment

We acknowledge the financial support provided by the National Science Foundation CBET-2215421 and CMMI-2001207.

Appendix A. Supplementary data

Supplementary data to this article can be found online at https://doi.org/10.1016/j.enbuild.2024.114926.

Data availability

Data will be made available on request.

References

[1] T.R. Oke, Boundary Layer Climates, Methuen, 1978.
[2] A.M. Rizwan, L.Y.C. Dennis, C. Liu, A review on the generation, determination and mitigation of Urban Heat Island, J. Environ. Sci. 20 (1) (2008) 120–128, https://doi.org/10.1016/S1001-0742(08)60019-4.
[3] A. Salvati, M. Kolokotroni, A. Kotopouleas, R. Watkins, R. Giridharan, M. Nikolopoulou, Impact of reflective materials on urban canyon albedo, outdoor and indoor microclimates, Build. Environ. 207 (2022) 108459, https://doi.org/10.1016/j.buildenv.2021.108459.
[4] J. Wen, M. Ignatius, E.X. Chen, N.H. Wong, Impacts of a highly reflective stainless-steel façade on a surrounding building: a case study in Singapore, Sustain. Cities Soc. 90 (2023) 104377, https://doi.org/10.1016/j.scs.2022.104377.
[5] 'Death ray' at Vegas hotel pool heats up guests, NBC News. Accessed: Jan. 29, 2024. [Online]. Available: https://www.nbcnews.com/id/wbna39403349.
[6] R. Wotzak, Window Reflections Can Melt Vinyl Siding, GreenBuildingAdvisor. Accessed: Jan. 29, 2024. [Online]. Available: https://www.greenbuildingadvisor.com/article/window-reflections-can-melt-vinyl-siding.
[7] S. Somasundaram, S.R. Thangavelu, A. Chong, Improving building efficiency using low-e coating based retrofit double glazing with solar films, Appl. Therm. Eng. 171 (2020) 115064, https://doi.org/10.1016/j.applthermaleng.2020.115064.

[8] R. and M. ltd, Low-E Glass: Global Strategic Business Report – Research and Markets. Accessed: Mar. 18, 2023. [Online]. Available: https://www.researchandmarkets.com/reports/5140383/low-e-glass-global-strategic-business-report.
[9] J. Yang, Z. Xu, H. Ye, X. Xu, X. Wu, J. Wang, Performance analyses of building energy on phase transition processes of VO2 windows with an improved model, Appl. Energy 159 (Dec. 2015) 502–508, https://doi.org/10.1016/j.apenergy.2015.08.130.
[10] Y. Sun, et al., Energy and daylight performance of a smart window: Window integrated with thermotropic parallel slat-transparent insulation material, Appl. Energy 293 (2021) 116826, https://doi.org/10.1016/j.apenergy.2021.116826.
[11] J.J. Wang, D. Shi, Spectral selective and photothermal nano structured thin films for energy efficient windows, Appl. Energy 208 (2017) 83–96.
[12] E. Zhang, Q. Duan, J. Wang, Y. Zhao, Y. Feng, Experimental and numerical analysis of the energy performance of building windows with solar NIR-driven plasmonic photothermal effects, Energ. Conver. Manage. 245 (2021) 114594, https://doi.org/10.1016/j.enconman.2021.114594.
[13] H. Akbari, H.D. Matthews, Global cooling updates: reflective roofs and pavements, Energ. Build. 55 (2012) 2–6, https://doi.org/10.1016/j.enbuild.2012.02.055.
[14] J. Yuan, C. Farnham, K. Emura, Effect of different reflection directional characteristics of building facades on outdoor thermal environment and indoor heat loads by CFD analysis, Urban Clim. 38 (2021) 100875, https://doi.org/10.1016/j.uclim.2021.100875.
[15] T.A.L. Martins, et al., Impact of Urban Cool Island measures on outdoor climate and pedestrian comfort: simulations for a new district of Toulouse, France, Sustain. Cities Soc. 26 (2016) 9–26, https://doi.org/10.1016/j.scs.2016.05.003.
[16] K. Mehaoued, B. Lartigue, Influence of a reflective glass façade on surrounding microclimate and building cooling load: case of an office building in Algiers, Sustain. Cities Soc. 46 (2019) 101443, https://doi.org/10.1016/j.scs.2019.101443.
[17] J. Zhang, Z. Li, Y. Wei, D. Hu, Influences of the window size and reflectivity on surrounding thermal environment, Appl. Energy 357 (2024) 122536, https://doi.org/10.1016/j.apenergy.2023.122536.
[18] B. Castellani, A.M. Gambelli, A. Nicolini, F. Rossi, Optic-energy and visual comfort analysis of retro-reflective building plasters, Build. Environ. 174 (2020) 106781, https://doi.org/10.1016/j.buildenv.2020.106781.
[19] F. Rossi, et al., Retroreflective façades for urban heat island mitigation: experimental investigation and energy evaluations, Appl. Energy 145 (2015) 8–20, https://doi.org/10.1016/j.apenergy.2015.01.129.
[20] S.W. Kim, R.D. Brown, Urban heat island (UHI) variations within a city boundary: a systematic literature review, Renew. Sustain. Energy Rev. 148 (2021) 111256, https://doi.org/10.1016/j.rser.2021.111256.
[21] C. Yang, et al., Assessing the effects of 2D/3D urban morphology on the 3D urban thermal environment by using multi-source remote sensing data and UAV measurements: a case study of the snow-climate city of Changchun, China, J. Clean. Prod. 321 (2021) 128956, https://doi.org/10.1016/j.jclepro.2021.128956.
[22] G. Evola, V. Costanzo, C. Magrì, G. Margani, L. Marletta, E. Naboni, A novel comprehensive workflow for modelling outdoor thermal comfort and energy demand in urban canyons: results and critical issues, Energ. Buildings 216 (2020) 109946, https://doi.org/10.1016/j.enbuild.2020.109946.
[23] P.A. Mirzaei, Recent challenges in modeling of urban heat island, Sustain. Cities Soc. 19 (2015) 200–206, https://doi.org/10.1016/j.scs.2015.04.001.
[24] E. Bashir, M. Luštrek, Intelligent Environments 2021: Workshop Proceedings of the 17th International Conference on Intelligent Environments, IOS Press, 2021.
[25] M. Taleghani, P.J. Crank, A. Mohegh, D.J. Sailor, G.A. Ban-Weiss, The impact of heat mitigation strategies on the energy balance of a neighborhood in Los Angeles, Sol. Energy 177 (2019) 604–611, https://doi.org/10.1016/j.solener.2018.11.041.
[26] S. Shooshtarian, C.K.C. Lam, I. Kenawy, Outdoor thermal comfort assessment: a review on thermal comfort research in Australia, Build. Environ. 177 (2020) 106917, https://doi.org/10.1016/j.buildenv.2020.106917.
[27] S. Liu, J. Zhang, J. Li, Y. Li, J. Zhang, X. Wu, Simulating and mitigating extreme urban heat island effects in a factory area based on machine learning, Build. Environ. 202 (2021) 108051, https://doi.org/10.1016/j.buildenv.2021.108051.
[28] J. Mendez-Astudillo, M. Mendez-Astudillo, A machine learning approach to monitoring the UHI from GNSS data, IEEE Trans. Geosci. Remote Sens. 60 (2022) 1–11, https://doi.org/10.1109/TGRS.2021.3091949.
[29] G.M. Stavrakakis, D.A. Katsaprakakis, M. Damasiotis, Basic principles, most common computational tools, and capabilities for building energy and urban microclimate simulations, Energies 14(20) (2021) 20. doi: 10.3390/en14206707.
[30] Z. Liu, W. Cheng, C.Y. Jim, T.E. Morakinyo, Y. Shi, E. Ng, Heat mitigation benefits of urban green and blue infrastructures: a systematic review of modeling techniques, validation and scenario simulation in ENVI-met V4, Build. Environ. 200 (2021) 107939, https://doi.org/10.1016/j.buildenv.2021.107939.
[31] Elk, Food4Rhino. Accessed: Feb. 25, 2023. [Online]. Available: https://www.food4rhino.com/en/app/elk.
[32] Heat Response: Creative Action for Philly's Rising Temperatures – Our Work in PA, Trust for Public Land. Accessed: Jan. 31, 2024. [Online]. Available: https://www.tpl.org/our-work/philadelphia-heat-response.
[33] Philadelphia Heat Vulnerability Index. Accessed: Jan. 31, 2024. [Online]. Available: https://phl.maps.arcgis.com/apps/webappviewer/index.html?id=9ef74cdc0c83455c9df031c868083efd.
[34] Google Earth. Accessed: Mar. 31, 2023. [Online]. Available: https://earth.google.com/web/search/Logan+Square,+Philadelphia,+PA/@39.95531348,-75.16991861,5.37579342a,1043.8453704d,35y,-10.39534125h,11.98353342t,0r/data=CigiJgokCZdajKsEZkRAESyh1S5nZURAGczxpffRdlPAIdikUYuOd1PA.
[35] C. Rosenzweig, et al., Mitigating New York City's heat island with urban forestry, living roofs, and light surfaces.
[36] H. Akbari, S. Konopacki, Calculating energy-saving potentials of heat-island reduction strategies, Energy Policy 33 (6) (2005) 721–756, https://doi.org/10.1016/j.enpol.2003.10.001.
[37] O. US EPA, Reduce Urban Heat Island Effect. Accessed: Mar. 15, 2023. [Online]. Available: https://www.epa.gov/green-infrastructure/reduce-urban-heat-island-effect.
[38] C. Curcija, S. Vidanovic, R. Hart, J. Jonsson, R. Mitchell, WINDOW Technical Documentation, 2018.
[39] M. Ichinose, T. Inoue, T. Nagahama, Effect of retro-reflecting transparent window on anthropogenic urban heat balance, Energ. Buildings 157 (2017) 157–165, https://doi.org/10.1016/j.enbuild.2017.01.051.
[40] T.T. Smith, B.F. Zaitchik, J.M. Gohlke, Heat waves in the United States: definitions, patterns and trends, Clim. Change 118 (3–4) (2013) 811–825, https://doi.org/10.1007/s10584-012-0659-2.
[41] Digital Codes. Accessed: Jan. 31, 2024. [Online]. Available: https://codes.iccsafe.org/content/IECC2018P5.
[42] T. Charan, et al., Integration of open-source URBANopt and dragonfly energy modeling capabilities into practitioner workflows for district-scale planning and design, Energies 14(18) (2021) 18. doi: 10.3390/en14185931.
[43] M. Krarti, P.M. Erickson, T.C. Hillman, A simplified method to estimate energy savings of artificial lighting use from daylighting, Build. Environ. 40 (6) (2005) 747–754, https://doi.org/10.1016/j.buildenv.2004.08.007.
[44] S. Zare, N. Hasheminejad, H.E. Shirvan, R. Hemmatjo, K. Sarebanzadeh, S. Ahmadi, Comparing Universal Thermal Climate Index (UTCI) with selected thermal indices/environmental parameters during 12 months of the year, Weather Clim. Extremes 19 (2018) 49–57, https://doi.org/10.1016/j.wace.2018.01.004.
[45] K. Błażejczyk, New climatological and physiological model of the human heat balance outdoor (MENEX) and its applications in bioclimatological studies in different scales, 28 (1994) 27–58.
[46] P. Bröde, et al., Deriving the operational procedure for the Universal Thermal Climate Index (UTCI), Int. J. Biometeorol. 56 (3) (2012) 481–494, https://doi.org/10.1007/s00484-011-0454-1.
[47] H. Farajzadeh, M. Saligheh, B. Alijani, Application of Universal Thermal Climate Index in Iran from tourism perspective, J. Nat. Environ. Hazards 5 (7) (2016) 117–138, https://doi.org/10.22111/jneh.2016.2658.
[48] E. Arens, T. Hoyt, X. Zhou, L. Huang, H. Zhang, S. Schiavon, Modeling the comfort effects of short-wave solar radiation indoors, Build. Environ. 88 (2015) 3–9, https://doi.org/10.1016/j.buildenv.2014.09.004.
[49] J.H. Yang, The curious case of urban heat island: a systems analysis, Thesis, Massachusetts Institute of Technology, 2016. Accessed: Mar. 16, 2023. [Online]. Available: https://dspace.mit.edu/handle/1721.1/107347.
[50] B. Bueno Unzeta, An urban weather generator coupling a building simulation program with an urban canopy model, Thesis, Massachusetts Institute of Technology, 2010. Accessed: Mar. 14, 2023. [Online]. Available: https://dspace.mit.edu/handle/1721.1/59107.
[51] A. Nakano, B. Bueno, L. Norford, C.F. Reinhart, Urban Weather Generator – A Novel Workflow for Integrating Urban Heat Island Effect within Urban Design Process, MIT web domain, Dec. 2015, Accessed: Mar. 16, 2023. [Online]. Available: https://dspace.mit.edu/handle/1721.1/108779.
[52] Run Urban Weather Generator. Accessed: Jan. 29, 2024. [Online]. Available: https://docs.ladybug.tools/dragonfly-primer/.
[53] A. Tseliou, E. Melas, A. Mela, I. Tsiros, Environmental impact of urban design elements in a Mediterranean City, Environ. Sci. Proc. 26(1) (2023) 1. doi: 10.3390/environsciproc2023026076.
[54] A. Salvati, M. Kolokotroni, Microclimate data for building energy modelling: study on ENVI-met forcing data, presented at the Building Simulation 2019, Rome, Italy, pp. 3361–3368. doi: 10.26868/25222708.2019.210544.